



1 **Evolution of the dynamics, area and ice production of the**
2 **Amundsen Sea Polynya, Antarctica, 2016-2021**

3 Grant J. Macdonald, Stephen F. Ackley and Alberto M. Mestas-Núñez

4 NASA Center for Advanced Measurements in Extreme Environments (CAMEE), University of Texas at San Antonio,
5 San Antonio, TX 78249, USA

6 *Correspondence to:* Grant J. Macdonald (grant.macdonald@utsa.edu)

7

8 **Abstract.** Polynyas are key sites of ice production during the winter and are important sites of biological activity
9 and carbon sequestration during the summer. The Amundsen Sea Polynya (ASP) is the fourth largest Antarctic po-
10 lynya, has recorded the highest primary productivity and lies in an embayment of key oceanographic significance.
11 However, knowledge of its dynamics, and of sub-annual variations in its area and ice production, is limited. In this
12 study we primarily utilize Sentinel-1 SAR imagery, sea ice concentration products and climate reanalysis data, along
13 with bathymetric data, to analyze the ASP over the period November 2016 - March 2021. Specifically, we analyze
14 (i) qualitative changes in the ASP's characteristics and dynamics, and quantitative changes in (ii) summer polynya
15 area, (iii) winter polynya area and ice production. From our analysis of SAR imagery we find that ice produced by
16 the ASP becomes stuck in the vicinity of the polynya and sometimes flows back into the polynya, contributing to its
17 closure and limiting further ice production. The polynya forms westward off a persistent chain of grounded icebergs
18 that are located at the site of a bathymetric high. Grounded icebergs also influence the outflow of ice and facilitate
19 the formation of a 'secondary polynya' at times. Additionally, unlike some polynyas, ice produced by the polynya
20 flows westward after formation, along the coast and into the neighboring sea sector. During the summer and early
21 winter, broader regional sea ice conditions can play an important role in the polynya. The polynya opens in all sum-
22 mers, but record-low sea ice conditions in 2016/17 cause it to become part of the open ocean. During the winter, an
23 average of 78% of ice production occurs in April-May and September-October, but large polynya events often asso-
24 ciated with high winds can cause ice production throughout the winter. While passive microwave data or daily sea
25 ice concentration products remain key for analyzing variations in polynya area and ice production, we find that the
26 ability to directly observe and qualitatively analyze the polynya at a high temporal and spatial resolution with Senti-
27 nel-1 imagery provides important insights about the behavior of the polynya that are not possible with those da-
28 tasetts.

29

30

31

32

33

34

35

36



37 1. Introduction

38 Coastal polynyas, or ‘latent heat polynyas’ (and henceforth referred to simply as ‘polynyas’), are sites of
39 open water surrounded by sea ice and land, glacier ice or fast ice (Armstrong, 1972; Tamura et al., 2008; Park et al.,
40 2018). These polynyas are distributed around the coast of Antarctica and are typically at fixed geographic locations
41 each year. They develop because the ice that forms at these sites is regularly driven away by winds or ocean cur-
42 rents, creating an opening in the sea ice (Bromwich and Kurtz, 1984; Bromwich et al., 1993; 1998; Morales
43 Maqueda et al. 2004; Sansiviero et al., 2017).

44 Between the Antarctic summer months of approximately November and March these open water sites tend
45 to remain persistently ice-free. Among other factors, the combination of ice-free conditions, summer sunlight, and
46 the availability of dissolved iron (e.g. Arrigo et al., 2008a; 2012; St-Laurent et al., 2017), enables large phytoplank-
47 ton blooms to develop in polynyas during this summer period. These phytoplankton blooms fix carbon from dis-
48 solved carbon dioxide, some of which then sinks below the surface layer (Sweeney et al., 2003). As a result, the
49 evolution of polynyas during the summer is considered a key factor in the primary productivity of the Southern
50 Ocean, and consequently, also their role in the sequestration of carbon dioxide (the ‘biological pump’) (Arrigo et al.,
51 2008b).

52 Between the Antarctic winter months of approximately April and October polynyas tend to intermittently
53 open and are smaller in area than in the summer. When a polynya does open during the winter, excess ocean heat is
54 lost and new sea ice production takes place in the opened area. Winds (usually katabatic winds) or ocean currents
55 then push the newly produced sea ice away and open the polynya again, producing yet more sea ice in the open area.
56 Repeated polynya ‘events’ produce new sea ice throughout the winter period and hence polynyas have been termed
57 ‘factories’ of sea ice production (Kimura and Wakatsuchi, 2004; Assmann et al., 2005). Overall, polynyas are esti-
58 mated to contribute around 10% of all Antarctic sea ice cover (Tamura et al., 2008; Nihashi and Oshima, 2015).
59 Regionally, polynyas can play an even larger role in production. For example, the Ross Ice Shelf polynya is estimat-
60 ed to produce several cubic kilometers of ice annually, and along with the McMurdo Sound Polynya, may produce
61 20-50% of total sea ice in the region (Drucker et al., 2011). The polynya-produced ice then forms part of the pack
62 ice, contributing to its characteristics and potentially further thickening due to deformation. For example, ice formed
63 by the Terra Nova Bay polynya in the Ross Sea had a mean thickness 3-4 times that of the central Ross Sea, with
64 80% of the study area’s ice contained in deformed ice and ridges (Rack et al., 2020). Consequently, understanding
65 of polynya evolution through the winter is important for understanding ice production and sea ice characteristics in
66 the Southern Ocean.

67 The Amundsen Sea Polynya (ASP), West Antarctica and the embayment in which it lies are of particular
68 interest for several reasons. The polynya is situated in the embayment into which the Thwaites and Pine Island Glac-
69 iers terminate and undergo ocean-driven melting, making the oceanography of the embayment of special interest
70 (IMBIE team, 2018; Rignot et al., 2019). The ASP is also known to be a key site of primary productivity in the
71 summer, supporting rates of net primary production up to $2.5\text{gC m}^{-2}\text{ day}^{-1}$, the highest for any Antarctic polynya
72 (Arrigo and Van Dijken, 2003; Arrigo et al., 2012), although the level of associated carbon sequestration is unclear
73 (Lee et al., 2017; St-Laurent et al., 2019). Additionally, the ASP has been highlighted as an important site for ice



74 production. It has been identified as the fourth highest polynya in Antarctica in terms of area and ice production,
75 only behind the Ross Ice Shelf, Cape Damley, and Mertz polynyas (Tamura et al., 2008; 2016; Nihashi and
76 Ohshima, 2015, Nihashi et al., 2017).

77 While there have been several recent studies of the ASP's evolution during the summer months (e.g. Arrigo
78 et al., 2012; Stammerjohn et al., 2015, St-Laurent et al., 2019), knowledge of the ASP and its role in ice production
79 during the winter is limited. Additionally, few studies during the summer have analyzed changes at the sub-monthly
80 scale, and none have observed the polynya directly during cloudy conditions. Aside from one study that analyzed the
81 ASP at the mean monthly scale (Tamura et al., 2016), studies that analyze ice production in the ASP during the win-
82 ter have been limited to estimates of total annual ice production and mean annual area as part of broader-scale cir-
83 cum-Antarctic studies (Tamura et al., 2008; Nihashi and Ohshima, 2015; Nihashi et al., 2017). Other studies of the
84 ASP during the winter have focused on other aspects of the polynya, such as iron and carbon fluxes (St-Laurent et
85 al., 2019). There is a lack of studies of the polynya that characterize changes in the polynya's evolution and area
86 through individual seasons. This is partly due to the difficulty of analyzing polynyas in detail during the polar night.
87 However, the launch of the Sentinel-1 constellation of Synthetic Aperture Radar (SAR) - in full operation by May
88 2016 - enables us to directly observe the polynya during the polar night at a high spatial resolution. Additionally,
89 during the summer light, SAR allows us to make observations regardless of cloud cover.

90 The overall goal of the work presented here is to improve knowledge of the behavior and evolution of the
91 ASP, and thus to aid understanding of recent complex and poorly understood trends in Southern Ocean sea ice con-
92 ditions. This in turn, will aid projections of future changes in Southern Ocean sea condition due to climate change,
93 with important consequences for a range of processes such as Antarctic Ice Sheet stability (Banwell et al., 2017;
94 Webber et al., 2017; Greene et al., 2018; Massom et al., 2018; Arthur et al., 2021) and ecosystem productivity
95 (Grossman and Dieckmann, 1994; Ito et al., 2017). In particular we aim to provide the first qualitative description
96 of the polynya's behavior based on direct observation. The three specific objectives of this paper are to, over the
97 period November 2016 - March 2021, analyze seasonal and inter-annual (i) qualitative changes in the ASP's charac-
98 teristics and dynamics, and quantitative changes in (ii) summer polynya area and (iii) winter polynya area and ice
99 production. The main datasets used are Sentinel-1 SAR images, sea ice concentration products, and climate reanaly-
100 sis data in the region of the ASP. Additionally, we analyze bathymetric data, and changes in the broader regional sea
101 ice.

102

103 **2. Study Site**

104 The ASP is located at around ~72-73°S and 110-120°W in the Amundsen Sea embayment of the Southern
105 Ocean in West Antarctica (Fig. 1). It is situated in a sector that exhibited an anomalous 40-year decreasing trend in
106 sea ice extent until a 2007 minimum, since which there has been an increasing trend (Parkinson, 2019). The embay-
107 ment also hosts an abundance of icebergs (Mazur et al., 2017; 2019; Bett et al., 2020). To the east, the polynya is
108 bound by the Thwaites Iceberg Tongue (Iceberg B22A; Budge and Long, 2018) and a chain of icebergs grounded
109 over Bear Ridge. To the south, when at its maximum extent, the polynya abuts the Dotson Ice Shelf and part of the
110 Getz Ice Shelf. Immediately east of the eastern boundary of the polynya is an area of ocean that is adjacent to



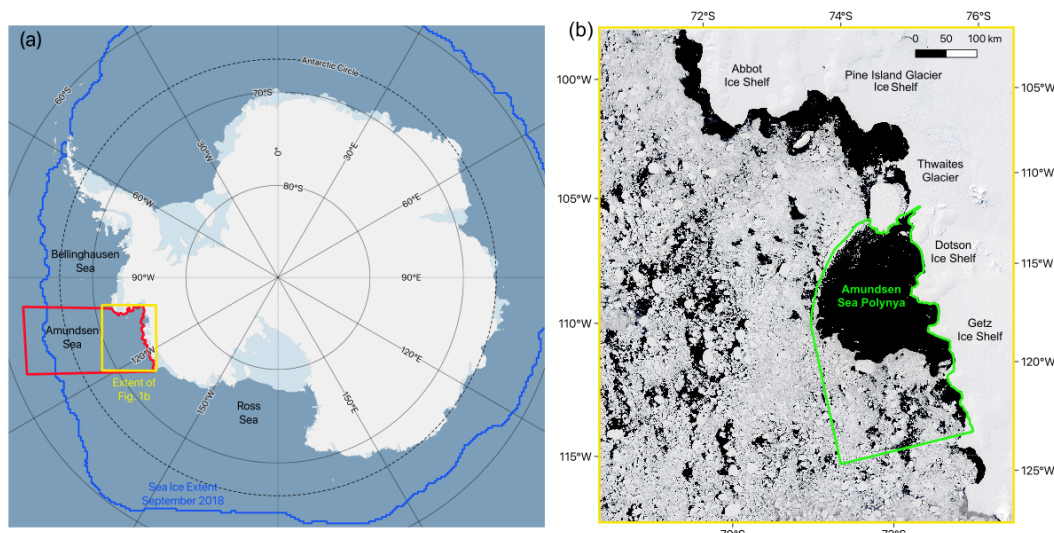
111 Thwaites Glacier and Pine Island Glacier. The neighboring ‘Pine Island Polynya’ forms along the coastal stretch
112 around this area and to the north. Westward coastal currents prevail in the area (Kim et al., 2016; St-Laurent et al.,
113 2019), that, along with easterly winds, carry icebergs (Koo et al., 2021) and sea ice into the adjacent sector or the
114 Amundsen Sea and eventually to the Ross Sea (Assmann et al., 2005).

115 The ASP opened every summer during the period 1979-2014 studied by Stammerjohn et al. (2015) and
116 retained some open polynya area through the winter period. Arrigo et al. (2012) found no significant secular trend in
117 mean summer open water area between 1997 and 2010, but Stammerjohn et al. (2015) did find the ASP’s area in
118 December-February to increase overall over the period 1979-2014. They also noted that the site of the polynya
119 opening shifted to its current typical site adjacent to the Thwaites Glacier Tongue in 1993, having previously been
120 further to the west.

121 Synoptic-scale winds have been found to primarily determine the ASP’s area and the timing of opening and
122 closure. Over the period 1997-2010, ASP area was greatest in the summers of 2002-03 and 2009-10, the years with
123 the largest monthly anomalies in easterly and southerly surface winds in the region, and smallest in 2003-04 when
124 there were anomalously high northerly and westerly winds (Arrigo et al., 2012). Polynya summer opening in No-
125 vember was associated with prevailing easterly or southeasterly winds, while closure in March was associated with
126 persistent southeasterly winds at a time when winds promote ice growth in open areas. The polynya was also found
127 to open for summer 16 ± 7 days earlier at the end of the period 1979/80-2013/14 than the beginning (Stammerjohn
128 et al., 2015).

129 During the winter, the polynya’s area was estimated to have a daily mean of 7700 ± 3600 km² for the peri-
130 od March-October, 2003-11, as estimated by mapping thin-ice thickness from Advanced Microwave Scanning Ra-
131 diometer for EOS [Earth Observing System] (AMSR-E) data (Nihashi and Ohshima, 2015). Annual ice production
132 volume has been estimated as 92 ± 16 km³ for the period 1992-2001 (Tamura et al., 2008) and 123 ± 24 km³ for the
133 period 1992-2013 (Tamura et al., 2016) by mapping thin-ice thickness using Special Sensor Microwave/Imager
134 (SSM/I) data and calculating heat flux using SSM/I and surface atmospheric data. Nihashi et al., 2017 estimated
135 annual volume of ice production, as 90 ± 13 km³ for the period 2003-10, and 90 ± 17 km³ for the period 2013-15, by
136 mapping thin-ice thickness and estimating heat fluxes using AMRS-E and AMSR2 data, respectively.

137



138
139 **Fig. 1.** (a) The location of the Amundsen Sea and our study sites within the context of Antarctica and the Southern
140 Ocean. The background image is from Quantarctica (Matsuoka et al., 2021); (b) The location of the ASP within the
141 Amundsen Sea embayment. The green boundary indicates the area defined as the ‘ASP study area’ for the purpose
142 of calculating winter polynya area and ice production. The background image is a true-color MODIS image from 12
143 December 2020.
144

145 3. Data & Methods

146 3.1 Qualitative analysis of the ASP’s evolution

147 In order to qualitatively characterize the seasonal and interannual evolution of the ASP we use Sentinel-1
148 SAR imagery. Sentinel-1 is a constellation of two satellites, A and B, that were launched by the European Space
149 Agency (ESA) in 2014 and 2016, respectively. The satellite collects radar backscatter imagery in the C-band which
150 allows observations of sea ice and the ocean during cloudy conditions and the polar night.

151 For our analysis we processed all Sentinel-1 extra-wide swath (EW) mode, Ground Range Detected (GRD)
152 images over the study site described in section 2 and its surroundings for the period November 2016 to March 2021.
153 This period was chosen because it includes all the complete summer (November-March) and winter (April-October)
154 periods during which both satellites A and B of the Sentinel-1 SAR constellation have been active. The EW mode
155 was primarily designed for sea ice and polar zones and collects images over a wider area than other modes. EW im-
156 ages are available in 20m x 40m spatial resolution and all images were resampled to 40 m grid spacing. Of four
157 available band combinations (VV, HH, VV+VH, and HH+HV), we use the HH band because most of the images
158 contain this band. Using these images, we created a time-lapse animation using Google Earth Engine. This time-
159 lapse included at least partial coverage of the study area for 56 days in 2016, 359 days in 2017, 341 days in 2018,
160 317 days in 2019, 329 days in 2020 and 85 days in 2021. In order to analyze particular images in detail, the images
161 were also downloaded from the Alaska Satellite Facility (asf.alaska.edu) and processed in ESA’s ‘SNAP’ toolbox.
162 SNAP was used to crop the images, apply radiometric correction, speckle filtering and ellipsoid correction and con-
163 vert the images to decibel values. The images were then loaded into QGIS (QGIS.org, 2021) for analysis.



164 Qualitative analysis was carried out by visually analyzing the time-lapse videos and images of interest, not-
165 ing changes in the state of the polynya and ice in the region. Visual analysis is possible because of the distinct
166 backscatter signals and texture of open water and different types of sea ice. Numerous previous studies have noted
167 the ability to observe polynya activity and visually identify polynya opening and the drift of ice with SAR imagery
168 and Sentinel-1 in particular (e.g. Hollands and Dierking, 2016; Dai et al., 2020). Typically, open ocean water has a
169 low backscatter and appears dark, while thicker, older icepack has a relatively high backscatter and appears bright
170 and more granular (we refer to all ice not produced by the ASP as ‘pack ice’) (Fig. 2a-b). Recently-formed polynya-
171 produced ice has an intermediate backscatter (Fig. 2a). Frazil ice, that may form when a polynya opens up and the
172 open ocean begins to freeze, forms in distinct bands of varying brightness (Fig. 2c-d). Note that what we refer to as
173 ‘open’ polynya area during the winter will typically be filled with thin, newly-forming frazil ice.

174 Given the role grounded icebergs play in bounding the ASP, we also downloaded the ‘BedMachine Antarc-
175 tica V2’ sea floor topography dataset for our study area to examine alongside our qualitative analysis. This dataset
176 was downloaded from the NSIDC (<https://nsidc.org/data/nsidc-0756>) and has a grid spacing of 500 x 500 m
177 (Morlighem et al., 2020).

178 We also use our analysis of the imagery to assess the approximate day of summer polynya ‘opening’ and
179 ‘closing’. We deem the polynya to be open for the summer when the open polynya area is primarily free of active
180 ice production, and the day of summer closing to be when the whole open polynya is subject to ice production.

181

182 **3.2 Daily polynya area**

183 In order to analyze seasonal and interannual changes in polynya area in summer and winter, daily sea ice
184 concentration (SIC) for the study region was downloaded from the University of Bremen’s sea ice data center
185 (seaice.uni-bremen.de). The data was separated into five summer periods from November to March (2016/17,
186 2017/18, 2018/19, 2019/20 2020/21) and four winter periods from April to October (2017, 2018, 2019, 2020). This
187 time period was focused on because it coincides with the period for which there is Sentinel-1 A and B data. Follow-
188 ing other studies (e.g. Dai et al., 2020) during the winter we also use the term ‘open polynya’ for areas that we in-
189 clude in the polynya, where an opening has been created and new ice production is taking place. However, during
190 the winter we expect thin ice to immediately begin forming when an opening is created, and thus we note the area is
191 not truly ‘open’ ocean. We begin our winter period in April rather than March because analysis of the Sentinel-1
192 imagery suggests ice production is not active across the open polynya at the beginning of March. The sea ice con-
193 centration product was processed by the University of Bremen using the ARTIST Sea Ice (ASIC) algorithm (Spreen
194 et al, 2008) applied to AMSR-2 data. AMSR-2 was launched onboard the Japan Aerospace Exploration Agency’s
195 (JAXA) Global Change Observation Mission - Water (GCOM-W) satellite in July 2012.

196 We used version 5.4 of the Antarctic-wide, daily sea ice concentration product with no land mask, pro-
197 cessed to 3.125 km grid spacing. This is of a higher-resolution than data previously used to analyze polynya area in
198 the region. For example, Arrigo et al., (2012) used SSM/I data with 6.25 km grid spacing for their study of summer
199 polynya area. Nihashi et al. (2017) used AMSR-E data with 6.25 km grid spacing for their estimates of ice produc-
200 tion. Tamura et al. (2008; 2016) also used SSM/I data, with 12.5 km grid spacing, for estimates of ice production.



201 Stammerjohn et al. (2015) used Bootstrap SIC data with 25 km grid spacing for their analysis of summer polynya
202 area. However, with our higher-resolution data (3.125 km) there remain limitations in using data with such a scale to
203 measure something that can vary on a meterscale. It has been estimated that the ice concentration error in our
204 AMSR-2 dataset is 25% at 0% SIC, decreasing to <10% error for SIC over 65% and 5.7% error at 100% SIC
205 (Spren et al., 2008). Data was available for all days in our study period apart from one day in 2019 (1 September).

206 After each day's data was downloaded as a geotiff, it was cropped to the 70 660 km² ASP study area de-
207 fined in Fig. 1b using a shapefile drawn in QGIS with a Sentinel-1 image as reference. Polynya area was then calcu-
208 lated by defining any pixel in the study area with a SIC < 70% as being part of the open polynya. The 70% threshold
209 has been commonly used in other studies of polynyas in the summer (e.g. Parmiggiani, 2006; Morelli & Parmiggia-
210 ni, 2013; Preußner et al., 2015), and the approach has also been used before to calculate winter polynya area (Cheng
211 et al., 2017; 2019). A limitation is that smaller areas of open water that are represented in a pixel dominated by ice-
212 covered area (i.e. > 70%) will not be included in our polynya area value, while ice-covered areas in pixels with SIC
213 < 70% will be included. However, by comparing our SIC data with the SAR imagery we found applying a 70%
214 threshold to the SIC data an effective way of capturing winter, as well as summer polynya area. For example, Fig. 2
215 b-d shows SAR imagery for a section of the polynya on 21-23 September 2020 and e-g shows the 'open' polynya as
216 identified using a 70% threshold with the SIC data for the same days. Observing Video S2 in comparison to availa-
217 ble images in Video S1 also shows how the SIC effectively captures polynya opening.

218 While Sentinel-1 imagery has been used to obtain polynya area during the polar night at a higher spatial
219 resolution (40m, Dai et al., 2020), the Bremen SIC product has three key advantages over using Sentinel-1 SAR
220 imagery. First, the SIC product is available daily, in contrast to Sentinel-1 which has many, and sometimes pro-
221 longed data gaps over the primary area of interest, particularly during June/July. Given that polynya area can change
222 substantially on a daily or hourly timescale, regular gaps of successive days significantly limits the ability to quanti-
223 tatively characterize variations throughout the year. Second, several Sentinel-1 images are required to capture the
224 whole ASP study area on a particular day, meaning that even on many days where there are images that are useful
225 for qualitative analysis, the whole polynya cannot be measured. For example, in 2020 there is full coverage for only
226 22 days with none between 26 April and 12 August. Third, even if sufficient images were available, current methods
227 for calculating polynya area in Sentinel-1 imagery (e.g. Dai et al., 2020) requires manual delimitation which is labor
228 intensive and would be highly time consuming to do for multiple years at a daily temporal resolution.

229

230 3.3 Daily winter ice production

231 In order to calculate daily ice production in the ASP during the winter periods we followed the approach of
232 Cheng et al. (2017) and utilized their heat flux and ice production model. As input to the model we used atmospheric
233 re-analysis data from the European Centre for Medium-Range Weather Forecasts Reanalysis v5 (ERA5) and the
234 same sea ice concentration data from the University of Bremen described in section 3.2.

235 Hourly ERA5 data, with a spatial resolution of 31 km, was downloaded from Copernicus
236 (cds.climate.copernicus.eu; Herbach et al., 2018) for the following meteorological variables: air temperature at a
237 height of 2 m, wind speed at a height of 10 m, surface air pressure, dewpoint temperature at a height of 2 m, down-



ward solar radiation and downward thermal radiation. Air temperature, wind speed, surface air pressure and dew-
point temperature were then processed to daily mean values, while solar and thermal radiation were processed to
daily cumulative values. These calculations were done for the same ASP study site as for polynya area (Fig. 1b).

241

242 3.3.1 Heat Flux Calculation

243 Following Cheng et al. (2017) the daily net heat flux, Q (in Wm^{-2}), of an open-polynya pixel was estimated
244 by:

245

$$246 Q = (1 - \alpha)R_i + L_i - L_o + F_s + F_e \quad (1)$$

247

248 where R_i (in Wm^{-2}) is the cumulative downward solar radiation; L_i (in Wm^{-2}) is the cumulative downward thermal
249 radiation; L_o (in Wm^{-2}) is the upward thermal radiation; F_s (in Wm^{-2}) and F_e (in Wm^{-2}) are the sensible heat flux
250 and latent heat flux, respectively; and α is the albedo of open water. α was taken to be 0.06 following Cheng et al.
251 (2017; 2019), R_i and L_i were taken from the processed daily ERA5 values and L_o , F_s and F_e were calculated as de-
252 scribed below.

253 The upward thermal radiation was calculated by the Stefan-Boltzmann law:

254

$$255 L_o = \varepsilon\sigma T_s^4 \quad (2)$$

256

257 where ε is the longwave emissivity of open water (0.99), and σ is the Stefan–Boltzmann constant (5.67×10^{-8}
258 $\text{W}^{-2}\text{K}^{-4}$). T_0 (in K), the freezing point of seawater, was assumed to be the temperature of the water surface (T_s , in K),
259 which was calculated following Doherty and Kester (1974) and Cheng et al. (2017; 2019) as:

260

$$261 T_s \sim T_0 = 273.15 - 0.0137 - 0.05199Sw - 0.00007225Sw^2 \quad (3)$$

262

263 where Sw (in ‰) is the salinity of sea water. The salinity of the Amundsen Sea was estimated as 34‰ based on Bett
264 et al. (2020).

265 The sensible heat flux, (F_s), and latent heat flux, (F_e) was calculated by:

266

$$267 F_s = \rho_a c_p C_s U (T_a - T_0) \quad (4)$$

268

269 and

270

$$271 F_e = 0.622\rho_a L_v C_e U (r_{e_a} - e_s)/P_0 \quad (5)$$

272

273 where ρ_a is the density of air at standard atmospheric pressure and 0°C, taken as, 1.3 kg m^{-3} , c_p is the specific heat
274 of air at constant pressure, taken as $1004 \text{ J kg}^{-1} \text{ K}^{-1}$, U (in ms^{-1}) is the wind speed at 10 m, taken from the processed



275 ERA5 data and T_a (in K) is the air temperature at 2 m, taken from the processed ERA5 data. C_s and C_e are bulk
276 transfer coefficients for sensible heat and latent heat, respectively and both taken as 0.00144. P_0 (in Pa) is the sur-
277 face air pressure and taken from the processed ERA5 data. L_v (in J kg^{-1}) is the latent heat of water vaporization, r is
278 the relative humidity. e_a (in Pa) is the saturation water vapor pressure at the air temperature, re_a is the actual water
279 vapor pressure of the air and e_s (in Pa) is the saturated water vapor pressure at the surface temperature and are all
280 calculated below:

281

$$282 \quad L_v = [2.501 - 0.00237(T_s - 273.15)] \times 10^6 \quad (6),$$

283

$$284 \quad e_s = 6.11.21 \times 10^{9.8094(T_s - 273.15)/(T_s + 0.71)} \quad (7),$$

285

286 and

287

$$288 \quad re_a = 611.21 \times 10^{9.8094(T_d - 273.15)/(T_d + 0.71)} \quad (8)$$

289

290 where T_d is the dewpoint temperature taken from the processed ERA5 data.

291

292 3.3.2 Ice production calculation

293 The calculated daily heat flux was then cropped, re-aligned, resampled to a 3.125 km^2 grid and reprojected
294 to Antarctic Polar Stereographic using GDAL (Geospatial Data Abstraction Library) and QGIS to match the corre-
295 sponding sea ice concentration data. Next, where SIC was < 0.7 (i.e. pixels considered as part of open polynya) daily
296 ice production volume, V , was estimated in km^3 following Cheng et al. (2017) by the following equation (9). Alt-
297 hough ice production will also take place in non-polynya areas where there is ice cover, here we are only concerned
298 with ice production taking place in the open polynya.

299

$$300 \quad V = 3.125^2(1 - \text{SIC})Q/\rho_i L_f \quad (9)$$

301

302 where, as above, SIC is sea ice concentration (as a fraction) and Q is daily net heat flux in W m^{-2} , ρ_i is sea ice densi-
303 ty and taken as 920 kg m^{-3} and L_f is the latent heat of sea ice fusion in J kg^{-1} . L_f is calculated following Mohammed
304 and Nirmal (2015) and Cheng et al. (2017) by:

305

$$306 \quad L_f = 333400 - 2113(T_0 - 273.15) - 114S_i + 18040S_i/(T_0 - 273.15) + 3.35S_i(T_0 - 273.15) - 3.76(T_0 - 273.15)^2 \quad (10)$$

307

308 where S_i is the salinity of sea ice, taken as 6‰ following Cheng et al. (2017).

309 Caution should be used when interpreting the absolute numbers produced by the ice production model, par-
310 ticularly because the input data is reanalysis data not necessarily always representative of reality. This is so because
311 the re-analysis itself is a simulation sensitive to uncertain parameter settings, although it is partly corrected by as-



312 simulation of observational data (Cheng et al., 2017; 2019). Also note ERA5 includes a prescribed ‘sea ice area frac-
313 tion’ parameter that influences the interaction between the atmosphere and ocean in the reanalysis. Nevertheless, we
314 opted for this method due to the difficulty of directly measuring and tracking thin ice thickness in the polynya (e.g.
315 Tian et al., 2020) to estimate ice production, and the potential to compare our daily ice production results to results
316 obtained by the same model for the Ross Ice Shelf Polynya (Cheng et al., 2017; 2019).

317

318 **3.4 Broader spatial changes in SIC**

319 In order to assess changes in the ASP in the context of changes in SIC at a broader spatial scale, SIC was
320 analyzed for the larger area defined in Fig. 1a. The same SIC dataset described in section 2.2 to obtain polynya area
321 was cropped to the broader region. The daily data was plotted spatially for all available days 1 November 2016 - 31
322 March 2021, as shown in Video S2. Monthly mean SIC was also calculated for the whole period and plotted spatial-
323 ly. Additionally, the total SIC for each day was calculated by calculating the sum of all percentage SIC values in the
324 study region. These total SIC values should only be considered useful for analyzing relative changes in SIC in our
325 study period.

326

327 **3.5 Wind speed and direction**

328 In order to analyze the polynya’s behaviour, we also considered wind conditions. Although a thorough
329 analysis of wind-vector/ice property correlations is beyond the scope of the present paper, which is primarily fo-
330 cused on estimating and describing the variability of the polynya’s dynamics, area and ice production, we do consid-
331 er wind conditions to help inform our analysis of the polynya. Mean daily and annual wind speed and direction was
332 calculated from ERA5 wind data. Hourly zonal (u) and meridional (v) components of winds at a height of 10 m
333 were obtained from ERA5 and processed into daily and annual means for a region adjacent to the Dotson Ice Shelf
334 and iceberg chain where the polynya typically forms, identified in Fig. S1. Hourly wind speed in ms^{-1} , V , was calcu-
335 lated as

336

$$337 V = (u^2 + v^2)^{1/2} \quad (11)$$

338

339 where u and v are ERA5’s u and v 10 m wind products, respectively. Daily wind speed and direction was plotted
340 spatially for the whole study area, included as supplementary video Video S3, the mean annual wind speed and di-
341 rection was plotted spatially as Fig.9 and as a daily mean speed value for a smaller area where the polynya forms
342 from, shown by Fig. S1.

343 Unfortunately there is a lack of local observations of wind data, and the closest station in the United States
344 Antarctic Program’s database, on Bear Peninsula, lacks wind data for most of our study period. As a result, some
345 caution should be employed when considering these results. However, Bracegirdle (2013) and Stammerjohn et al.
346 (2015) note that data from ERA5’s predecessor ERA-I in the neighboring Bellingshausen Sea performed better than
347 other reanalysis products.

348



349 4. Results

350 In this section, we first summarize our qualitative analysis of the polynya dynamics using Sentinel-1 SAR
351 imagery (Video S1) of the ASP between November 2016 and March 2021 (Section 4.1). Second, we analyze quanti-
352 tative changes in summer (November - March) polynya area for the summers of 2016/17 to 2020/21 (Section 4.2).
353 Third, we analyze quantitative changes in winter (April - October) polynya area and winter ice production for the
354 winters of 2017 to 2020 (Section 4.3). Fourth, we analyze spatial and temporal variations in wind speed and how
355 they relate to polynya area (Section 4.4), and finally, we analyze broader regional patterns in sea ice concentration
356 for the period November 2016 - March 2021 (Section 4.5).

357

358 4.1 Qualitative analysis of ASP using Sentinel-1 SAR imagery

359 Typically in November or early December the polynya transitions from a winter into summer ‘mode’ as it
360 expands to the west and ice production ceases to take place in the open area i.e. the open polynya area is occupied
361 by open ocean rather than frazil or grease ice (Table 1, Video S1, e.g. Fig 1b). While the polynya’s eastern and
362 southern boundaries remain fixed at the Iceberg Chain and coast, respectively, at times during the summer the po-
363 lynya becomes unbound to the west and/or north, and consequently congruent with the open ocean. In the summers
364 of 2018/19 and 2019/20 it remains bound, but in 2016/17 and 2017/18 substantial openings develop in the pack ice
365 boundary. In the summer of 2016/17, particularly from December, the pack ice in the region is notably sparse in
366 comparison to the other years.

367 In February the pack ice around the polynya becomes more extensive and compact, predominantly due to
368 inflow from the Bellingshausen Sea in the north east. As the new pack ice flows into the area it reforms a west-
369 ern/northern boundary to the polynya in the years where a gap had opened, and in all years pushes the existing pack
370 to the east and south-east, reducing the polynya’s size. In the exceptionally low-pack ice summer of 2016/17, the
371 newly formed boundary of pack ice is remarkably narrow. In March in all years, new ice production can be seen
372 forming in parts of the polynya and is taking place across all of the polynya by the end of March or early April,
373 marking the polynya’s transition into winter ‘mode’ (Table 1).

374 Throughout the winter, polynya ‘events’ occur, with existing ice moving away, predominantly to the west
375 off the Iceberg Chain and Thwaites Iceberg Tongue, and new ice forming in the opening (e.g. Figs. 2c-e). On occa-
376 sion the polynya instead forms to north off the Dotson Ice Shelf. Between April and August the main polynya ap-
377 pears to primarily have its maximum extent confined to the area adjacent to the Dotson Ice Shelf. Observation of
378 available imagery of polynya events, along with observation of newly-formed polynya ice outflowing from the area,
379 suggests that there is relatively low ice production in these deep winter months. Early and late in the winter, polynya
380 events are sometimes larger, extending further to the west, and there appears to be more associated ice production.

381 After early winter (March/April), as the area becomes more densely covered by inflowing pack ice and
382 newly-formed polynya ice, obstructions occur that appear to limit the evacuation of polynya-produced ice from the
383 vicinity and limit growth of the polynya. Obstructions particularly take place around and adjacent to a group of per-
384 sistenty stuck icebergs around the center of the study area that we call the Central Grounded Icebergs around a sea-
385 floor high (Fig. 2a, h). New ice also sometimes becomes stuck (fast) directly adjacent to the south-west of this site

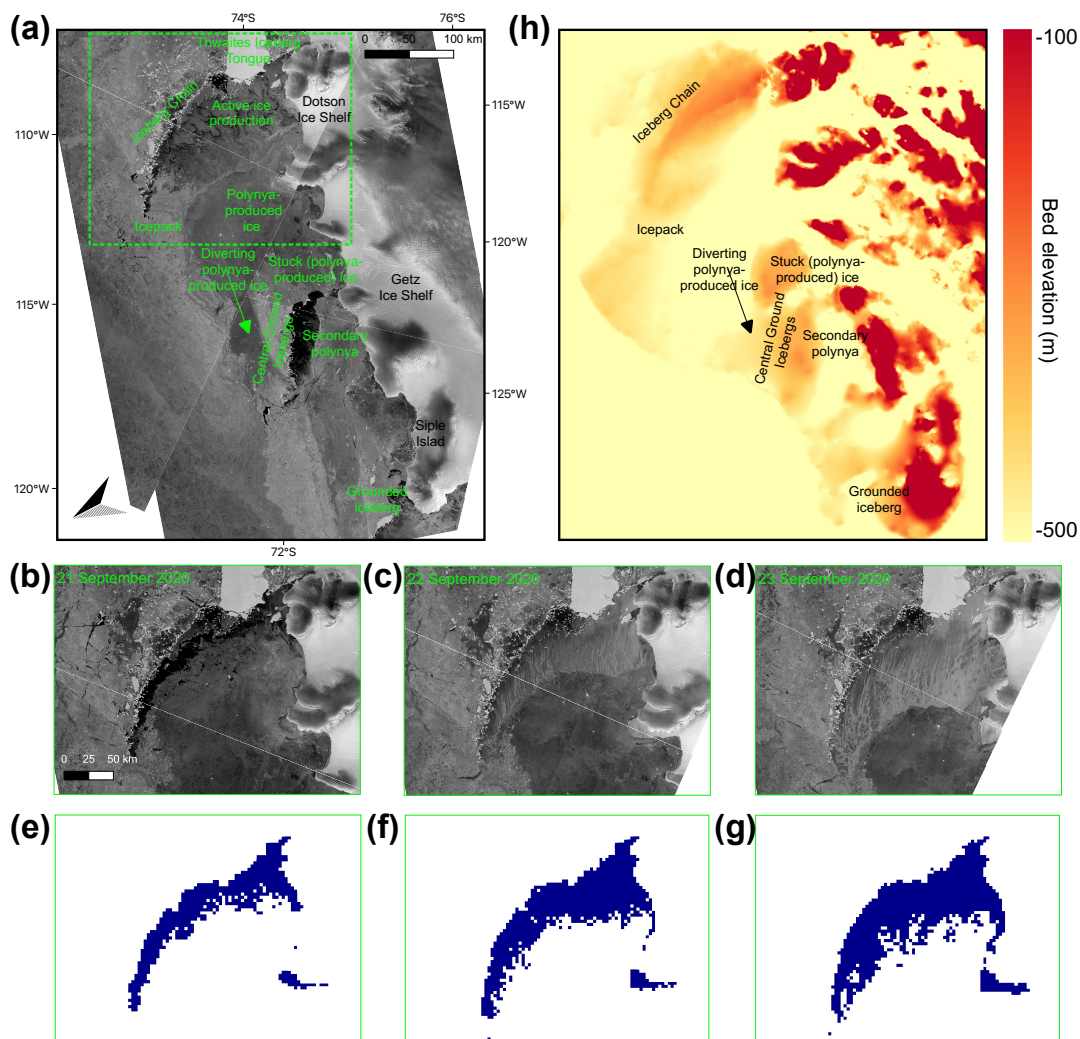


386 (Fig. 2a, h) on another sea-floor high. This intermittently-fast ice blocks outflow from the polynya to the west along
387 the coast, and at times forces new polynya-produced ice to divert around the north of Central Grounded Icebergs
388 (Fig. 2a). An area of grounded icebergs and intermittently-fast ice by Siple Island also sometimes obstructs ice and
389 causes diversions further to the north. All ice produced by the polynya flows to the west overall, eventually rounding
390 the corner of Siple Island.

391 We also observe that, while the overall flow of ice from the ASP is to the west, ice flowing from the polynya
392 through the winter ‘heaves’ and regularly temporarily reverses direction, ‘backfilling’ eastward into and towards
393 the polynya (e.g. Fig 3). This means the polynya sometimes closes through backfilling, and not only through for-
394 mation and growth of new ice. Back-filling also occur when the polynya does not appear open, meaning that rafting
395 and deformation presumably occurs as ice moves back into the polynya zone.

396 A series of smaller polynyas, other than the main polynya that forms off the Iceberg Chain and Dotson Ice
397 Shelf, also form within the study area at times. Mostly notably a ‘secondary polynya’ forms at times off the Central
398 Grounded Icebergs (Fig. 2a). With inflow of ice from the ASP to this area at times obstructed, as ice moves away
399 from the Central Grounded Icebergs to the west, an opening is created and active ice production is visible. Small
400 polynyas also form at times to the west off the outcrops along the coast.

401 By analyzing Video S1 it is sometimes possible to visually track ice produced by particular polynya events
402 through the season. In particular, in 2020, with some uncertainty due to missing images, we are able to estimate that
403 approximately all of the ice produced between 30 April and 4 November by the main polynya (i.e. excluding the
404 secondary polynya located by the Central Grounded Icebergs) is contained within the red outline on 4 November in
405 Fig. 4. This section of polynya-produced ice totals 46452 km² in area.



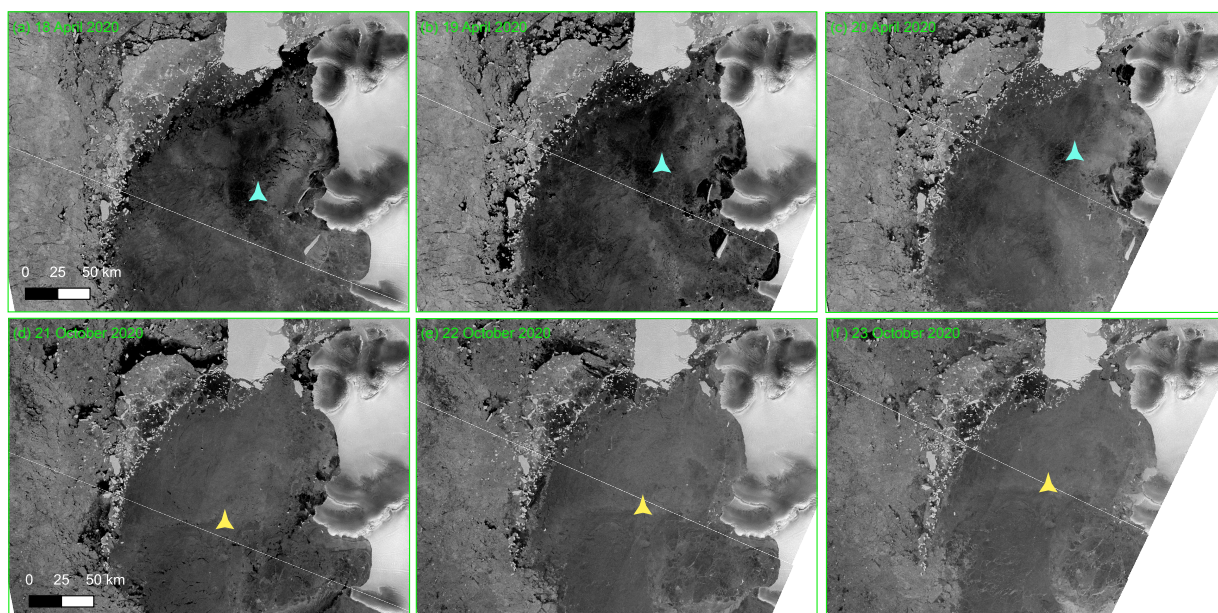
406
 407
 408 **Fig. 2.** (a) An example image of the ASP during the winter in a Sentinel-1 SAR image from 5 September 2019. (b-
 409 d) An example of a polynya event taking place 21-23 September 2020 in Sentinel-1 SAR imagery. Darker ice pro-
 410 duced by the ASP can be seen diverting around the Central Grounded Icebergs (and some fast pack ice) after ice
 411 became stuck and obstructed outflow along the coast. The area corresponds to the dashed-green box in (a). (e-g)
 412 Open polynya area (blue) for the same dates and areas as b-d as measured by using a 70% threshold with SIC data
 413 (h) The elevation of the bed referenced to mean sea level for the same area as (a). The bathymetry data is from the
 414 MEaSUREs BedMachine version 2 dataset (Morlighem et al., 2019).

415
 416



Year	Polynya opens	Polynya closes
2016/17	8 November 2016*	4 April 2017
2017/18	3 December 2017	9 March 2018
2018/19	13 November 2018	14 March 2019
2019/20	20 November 2019	21 March 2020
2020/21	16 November 2020	8 March 2021

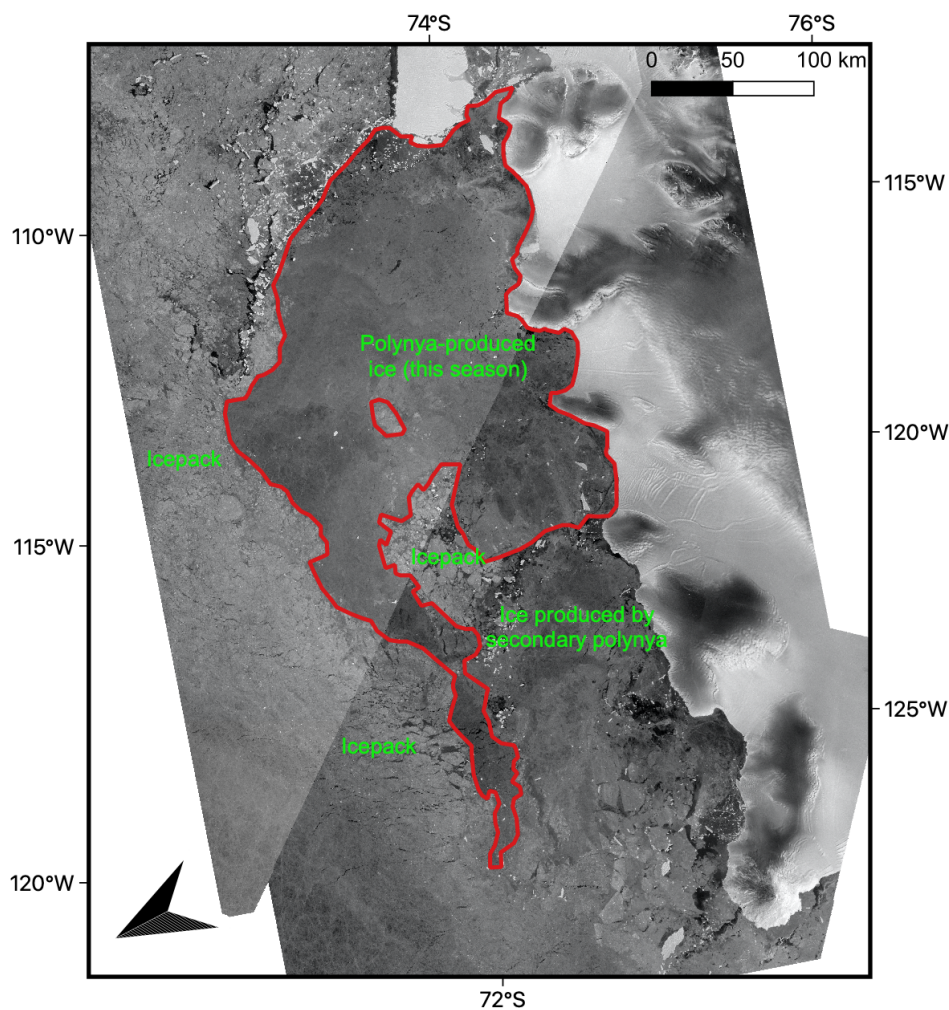
417
418 **Table 1.** Summer polynya opening and closing dates for each summer 2016/17-2020/21 as determined by visual
419 analysis of Sentinel-1 SAR imagery. We determine the polynya to be open for summer when the majority of the
420 open polynya is not exhibiting ice production and closed when the majority of the polynya is exhibiting ice produc-
421 tion. * in 2016/17 a lack of imagery in early November means it is difficult to determine when the polynya opened,
422 but it is open by 8 November.
423



424
425 **Fig. 3** Examples of 'back-filling', ice earlier produced by the ASP flowing back towards the area adjacent to the
426 Iceberg Chain where it formed. Each box corresponds to the same area shown by the dashed-green box in Fig. 2a,
427 (a-c) show the area on 18-20 April 2020, (d-f) show 21-23 October 2020. The colored shapes in each image are in
428 approximately the same relative position within the ice in each set of images and are to help the reader spot the



429 movement of the ice through the movement of adjacent features. Other examples of back-filling are visible in Video



430 S1.

431

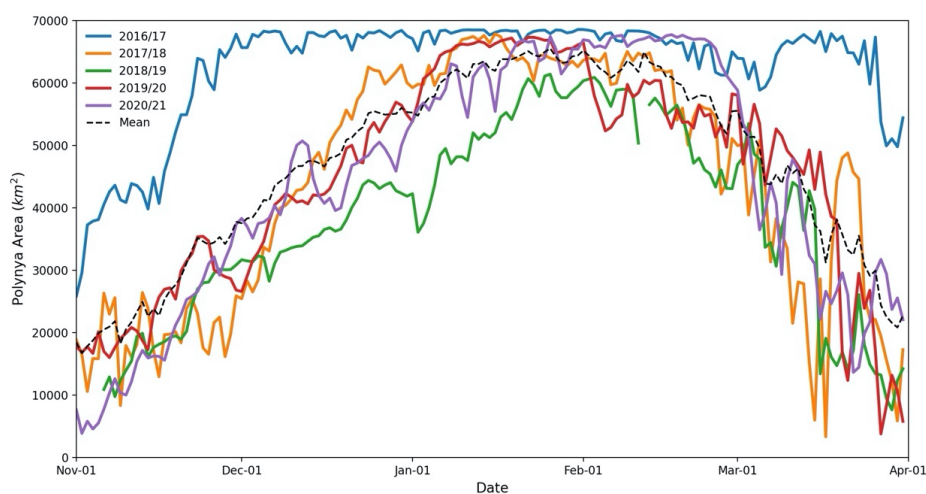
432

433 **Fig. 4.** Ice inside the red boundary is estimated, based on visual analysis of Video S1, to be approximately all the ice

434 produced by the main polynya between 30 April and 4 November 2020. Sentinel-1 SAR image from 4 November

435 2020.

436



437
438 **Fig. 5.** Daily summer (November-March) polynya area for each summer 2016/17-2020/21 (solid), and the daily
439 mean for the whole period (dashed).

440
441

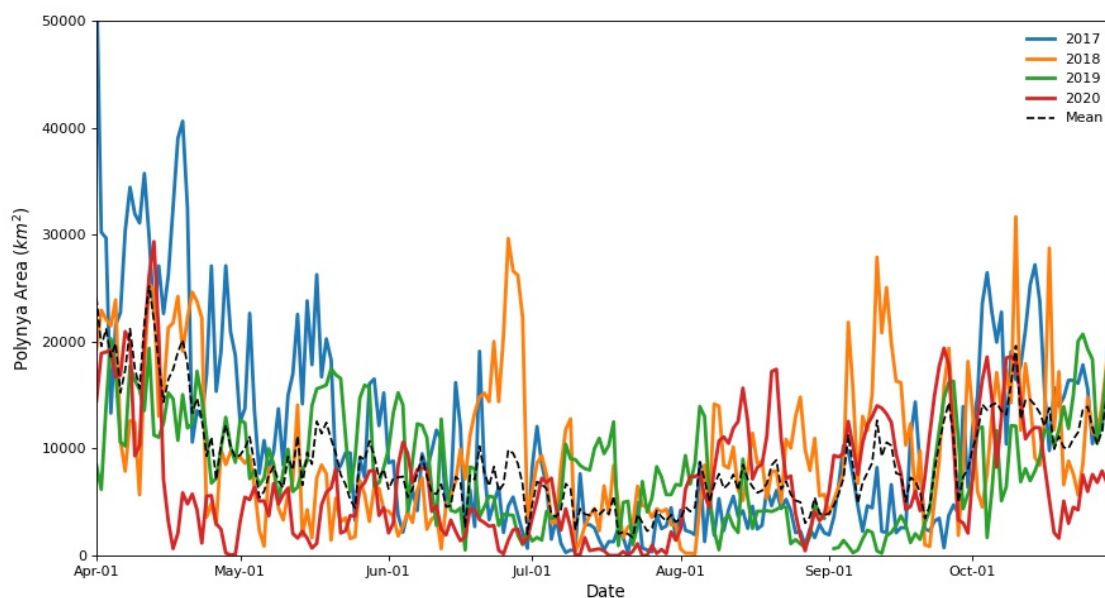
442 4.2 Summer Polynya Area

443 In all years there is an overall increase in polynya area through November (Fig 4). On 1 November, the
444 polynya has an area between 17 813 km² (2019) and 25 859 km² (2016). In the years 2017/18, 2018/19, 2019/20
445 and 2020/21 the polynya area then follows a similar pattern, but in 2016/17 it follows a distinct course. By 1 De-
446 cember in 2016 the polynya is open in approximately the whole ASP study area, with an area of 65 674 km², an in-
447 crease of 154% from 1 November. In 2016/17 the polynya remains open across approximately the whole study area
448 throughout December, January, and most of February and March, only beginning to significantly decline in late
449 March (Fig 4) and into April (Fig 5). The polynya in 2016/17 maintains a higher area than in all other years
450 throughout the whole summer, apart from a small period in late February when it is surpassed by 2020/21.

451 In 2017/18, 2018/19, 2020/21 and 2020/21 the polynya area has increased to between 25 439 km² (2017)
452 and 38 310 km² (2020) by 1 December. From then the polynya continues to follow an overall increasing trend
453 through December, with the polynya reaching its peak area in January in each of these years. In 2018/19 the peak
454 area is substantially lower (61 113 km²) than in other years, and the polynya only maintains an area above 60 000
455 km² for six days in late January and early February. 2018/19 records the lowest area in comparison to other years on
456 every day between 4 December and 3 February. In 2017/18, 2019/20 and 2020/21 the polynya behaves in a similar
457 manner through most the period, with no one of those years consistently recording a higher area, and each year
458 reaching a peak-open area that approximately fills the whole ASP study area. However, polynya area in 2020/21
459 reaches its peak later (January), and its decline begins later (late February). Notably, in 2017/18 the polynya experi-



460 ences a temporary rapid re-opening as it increases from just 5 977 km² on 15 March to 48 779 km² on 21 March.
461 This is an 82x increase in 6 days, and it is followed by a rapid decline. The polynya had the highest daily mean area
462 for summer (November-March) in 2016/17, at 62 616 km², and 2018/19 had the lowest, at 38 518 km². The mean
463 daily area of 2017/18, 2019/20 and 2020/21 for summer was 44 013 km², 44 979 km² and 44 447 km², respectively.



464
465 **Fig. 6.** Daily winter (April-October) polynya area for each winter 2017-2020 (solid), and the daily mean for the
466 whole period, as measured from AMSR-2 SIC data (dashed).

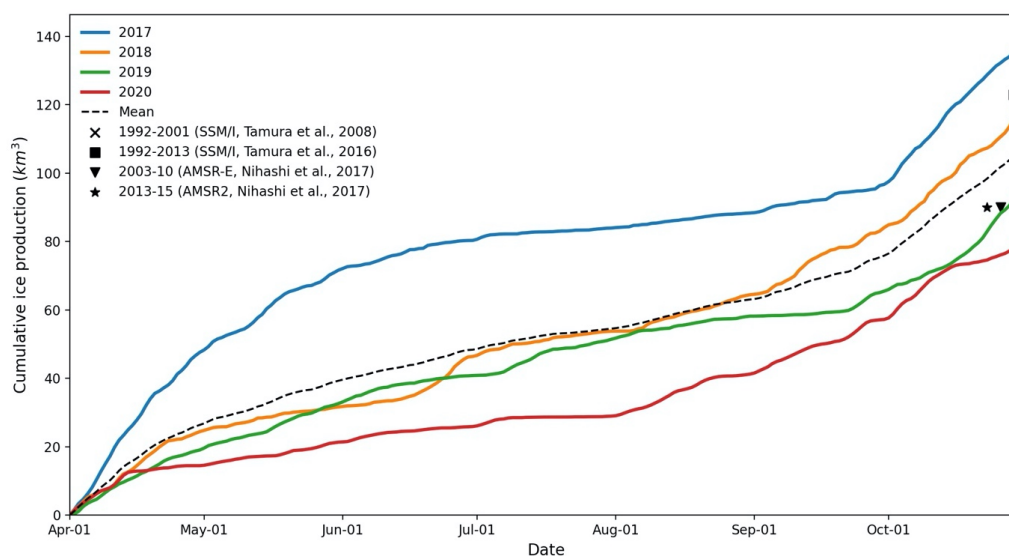
467
468 **4.3 Winter Polynya Area and Ice Production**

469 In all years, polynya area exhibits an overall decline from the beginning of the winter period, when the po-
470 lynya remains relatively large after the summer period (Fig. 6). This period, when the polynya remains relatively
471 large but ice production has now begun, accounts for a substantial proportion of the annual ice production (Fig. 7;
472 Fig. S2). On average, April/May accounts for 36% (39.6 km³) of annual ice production. The polynya then generally
473 reaches a sustained winter low in area, where it fluctuates around and below 10 000 km². In 2020 the polynya area
474 reaches its low in early April, while in 2017, 2019 and mean 2017-20 the area continues an overall decline through
475 April, May and June. Polynya area and ice production then tend to remain low until an increase begins around Sep-
476 tember. In July polynya area remains below 10 000 km² in all years for the whole month apart from brief small fluc-
477 tuations above this in 2018 and 2019. There are notable spikes in polynya area in the middle of the year, which are
478 also exhibited in spikes in ice production. Most notably in June in 2018 polynya area spikes to 26 631 km². After a
479 period of low polynya area, the area generally increases through September and October towards the summer period.
480 In 2020 this period of area and ice production increase begins in August. This late-winter increase in polynya area is
481 also exhibited in a corresponding marked increase in the rate of ice production. On average, September/October ac-
482 counts for 42% (45.8 km³) of annual ice production.



483 We note that in 2017 between the dates of 1 April and 8 May a substantial portion of the calculated open
484 polynya area, and ice production, occurs in the northwest of the ASP study area. This area is part of the open ocean
485 and is separated by sea ice from the more-typically open polynya area adjacent to the iceberg chain. Typically, ice-
486 pack fills this northwest area, but in early 2017 it is open due to the lack of icepack in this sector in the summer of
487 2016/17, discussed in section 4.3 (Video S2; Fig. 11b).

488 Analysis of the spatial distribution of ice production across all years reveals that the mean daily ice produc-
489 tion is highest in the area of the polynya adjacent to the Iceberg Chain, Thwaites Iceberg Tongue and Dotson Ice
490 Shelf (Fig. 8). Mean annual ice production values (April-October) in this region surpass $17 \text{ m}^3/\text{m}^2$. Other notable
491 areas of higher ice production lie along various parts of the coast and an area that corresponds to the secondary po-
492 lynya by the Central Grounded Icebergs.



493
494
495 **Fig. 7.** Daily cumulative winter ice production for each winter (April-October) 2017-2020 (solid), and the mean for
496 the period (dashed), as measured using heat-flux modeling of ERA-5 data and AMSR-2 SIC data. Also shown are
497 mean annual measurements for 1992-2001 (Tamura et al., 2008), 1992-2013 (Tamura et al., 2016), 2003-10 and
498 2013-15 (Nihashi et al., 2017), along with the instrument used for each measurement. Note the previous studies'
499 measurements covered the period March-October and used a study area that does not exactly correspond to ours.
500



Year	Mean Daily Polynya Area (km ²)	Total Annual Ice Production (km ³)	Total Mean Daily Ice Production (km ³)
2017	10 908 (9589)	139	0.67 (0.67)
2018	9 963 (7004)	121	0.57 (0.50)
2019	8 152 (5127)	95	0.45 (0.38)
2020	6 910 (5692)	80	0.38 (0.36)
Mean 2017-20	8 984 (7240)	109	0.52 (0.51)

Table 2. Estimates of Mean Daily Polynya Area, Total Annual Ice Production and Mean Daily Ice Production during the winters of 2017-2020, and for the daily mean of the period. Numbers in brackets indicate the standard deviation.

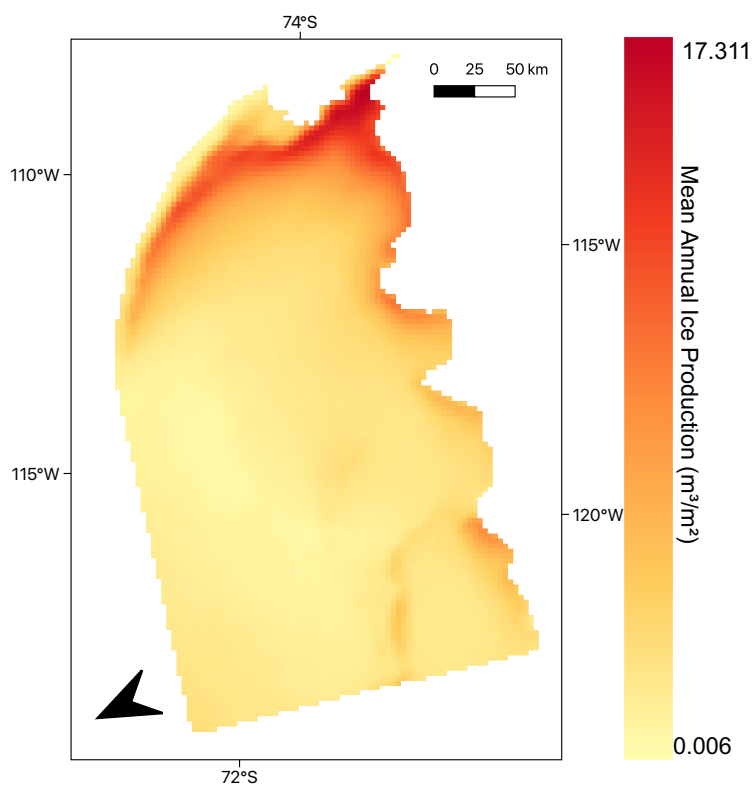


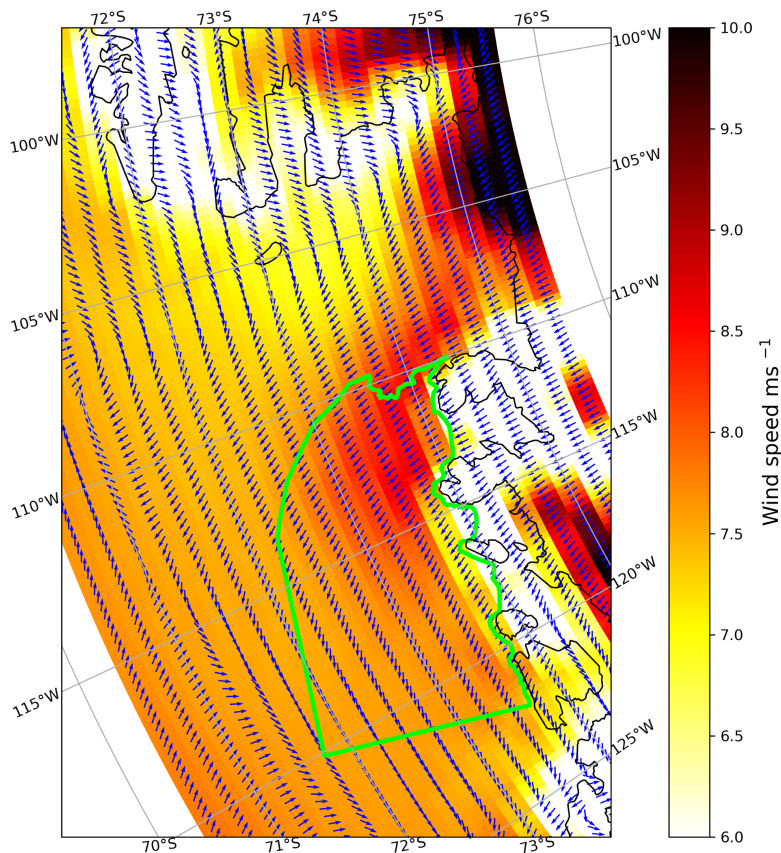
Fig. 8. Mean Annual Ice Production for all winter study periods (April-October 2017-2020). The region corresponds to the region within the green outline in Fig. 1b

501
 502



503 **4.4 Wind and polynya area**

504 Although it appears many day-to-day variations in polynya area are not correlated with wind speed, it is
505 clear that notable spikes in polynya area do often occur on days with high wind speed (Fig. S3), particularly when
506 there is an easterly component (Video S3). For example, the three highest polynya areas recorded in 2020 after April
507 all occur alongside the three highest spikes in wind speed post-April. By viewing the mean spatial distribution of
508 winds, it is clear that the ASP forms in an area of relatively high winds that often have an easterly component (Fig.
509 9). A band of high winds with a mean speed of around 8 - 9 ms⁻¹ exists along the coast from Thwaites Glacier, over
510 the Thwaites Iceberg Tongue and into the eastern area of the ASP study area, where the main polynya originates.
511

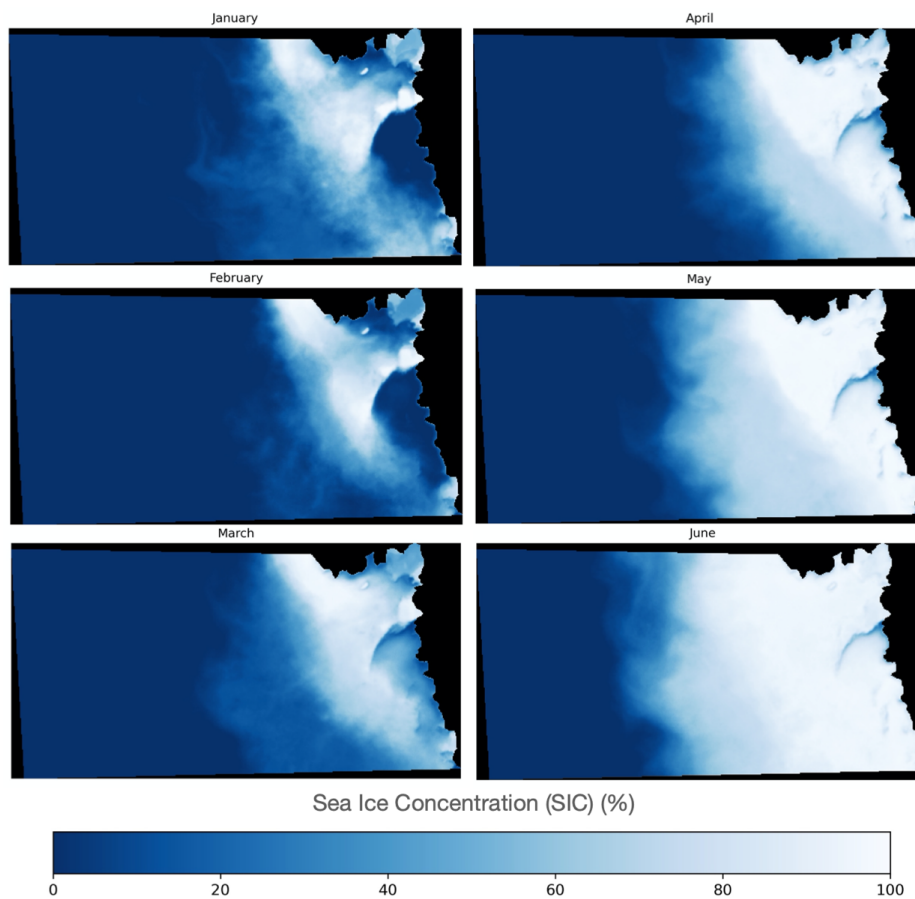


512
513
514
515
516
517
518

Fig. 9. Mean annual wind speed and direction, calculated for the period 1 November 2016 to 31 December 2020. The green box represents the ASP study area, the same as the green box in Fig 1b. Daily wind speed and direction is included as Video S3.



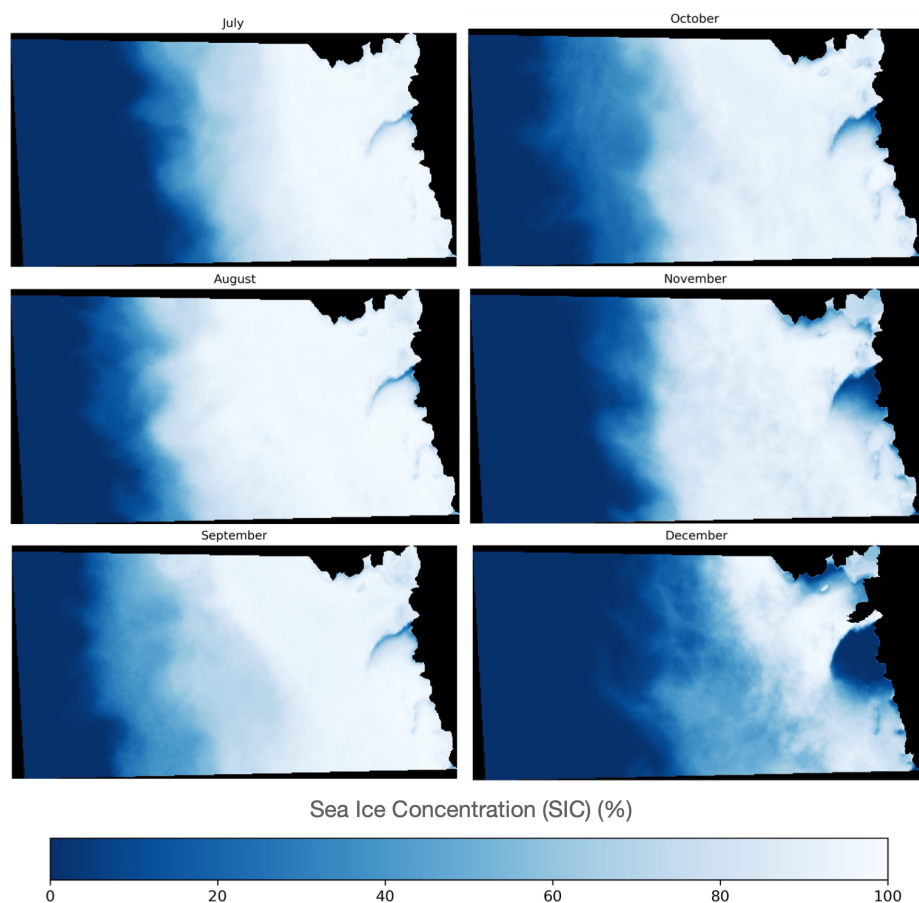
519
520



521
522
523
524
525
526
527
528
529
530
531
532

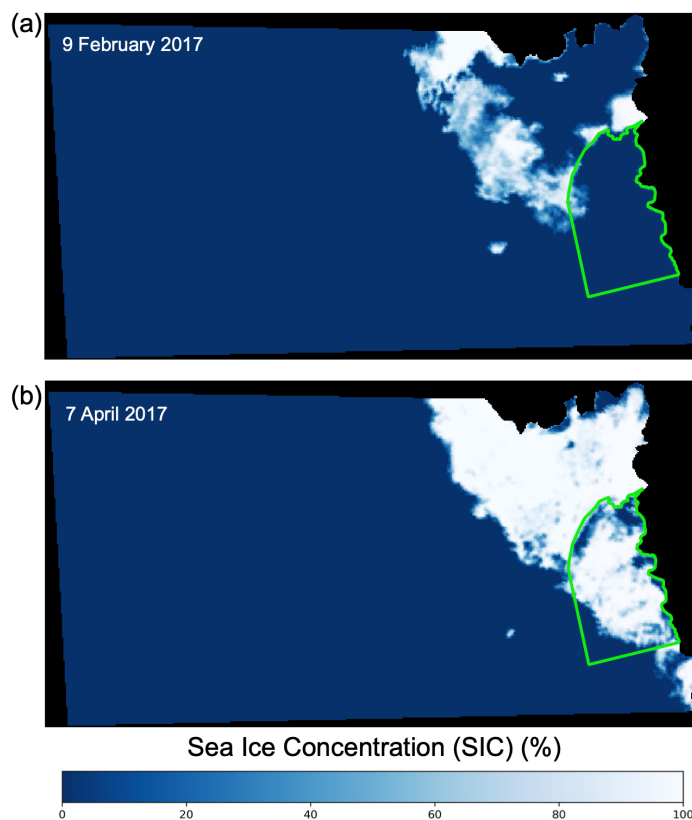


533
534



535
536
537
538
539
540
541
542
543
544

Fig. 10. Mean monthly SIC for the broader ASP region for the period November 2016 to March 2021. The area corresponds to that shown by red box in Fig. 1a. Daily data is shown in Video S2.



545

546

547 **Fig. 11.** SIC for the broader ASP region on two days in 2017, during and following a summer of record-low SIC. (a)
548 An example of when the polynya had no sea ice boundary to the west/north-west due to the exceptionally low SIC in
549 the region during the 2016/17 summer. (b) An example of the low SIC in the region early in the subsequent winter,
550 when only a narrow area of pack ice and polynya ice fills the area. The area corresponds to that shown by red box in
551 Fig. 1a.

552

553 4.5 Broader SIC

554 Analysis of the SIC over a broader area also shows daily changes in the polynya area and how it relates to
555 changes in the icepack. The mean monthly cycle of the polynya can be seen in Fig. 10 and presents a similar picture
556 of the polynya as described in sections 4.1- 4.3. The broader icepack has a minimum total SIC in January and re-
557 mains similar in February. From March the broader icepack can be seen to expand in area as the polynya begins to
558 close and continues to increase until a peak SIC in September. From October the icepack begins a marked decline
559 into summer. Interannual variation can be seen in Fig. S4 and Video S2, with maximum icepack area occurring in
560 August or September each year, and minimum icepack in January or February.



561 During the summer of 2016/17 the icepack is notably sparse (Fig. 11; S4). Around 29 December 2016 a
562 gap in the icepack connects the ASP to the open ocean to north. The icepack continues to diminish and the gap con-
563 necting the ASP to the open ocean broadens until by February the polynya is only bound by part of the Iceberg
564 Chain and Thwaites Iceberg Tongue. The total SIC reaches a minimum on 5 February 2017, 35% of the next lowest
565 annual minimum (2019/20). Gaps in icepack around the Iceberg Chain mean that the ASP has essentially joined
566 with the Pine Island Polynya through the Iceberg Chain for a period in this year. The narrow band of icepack from
567 the east closes the polynya off again in March but the band of adjacent icepack remains so narrow that, as men-
568 tioned, there is open ocean inside our ASP study area until 9 May (Video S2).

569

570 **5. Discussion**

571 Our analysis shows that in some ways the ASP, between November 2016 and March 2021, behaves as is
572 typical for Antarctic coastal polynyas. During the summer the polynya becomes larger and remains ice-free (Fig. 5,
573 Video S1), while during the winter it becomes smaller, opening up during ice-producing polynya ‘events’ (Figs. 5-6,
574 Video S1). These polynya events and changes in polynya area can sometimes be attributed to higher wind speeds
575 (Figs 8-9, S3).

576 Our qualitative analysis of Sentinel-1 SAR imagery, however, also reveals distinct characteristics of the
577 ASP which are not possible to decipher from sea ice concentration data, other quantitative methods, or indirect ob-
578 servation. First, we note that while in many other polynyas, such as the Ross Ice Shelf Polynya, new polynya-
579 produced ice is typically efficiently evacuated away from its origin (Dai et al., 2020), this is not the case at the ASP.
580 Instead, ice formed by the ASP often remains in the ASP study area for months (Video S1, Fig. 4). In fact, this po-
581 lynya-produced ice does not consistently flow in a direction away from the polynya. While its overall direction is
582 westward, away from the polynya, the ice ‘heaves’ and temporarily flows ‘backward’ (‘back-fills’) (Fig. 3), as has
583 also been observed at the Mertz Glacier Polynya (Massom et al., 2017). The ice also gets ‘stuck’ in the region, par-
584 ticularly around grounded icebergs, which are grounded in areas where there are topographic highs in the sea floor
585 (Fig. 2a, h).

586 The tendency of ice produced by the ASP to remain in the vicinity of the polynya for prolonged periods,
587 become stuck, and sometimes flow back eastward towards the site of its formation, influences the polynya and ice
588 production in two key ways. First, when ice moves eastward while the polynya is open it contributes to the closure
589 of the polynya, and thus the cessation of ice production. Typically, it is assumed that an open polynya during winter
590 closes due to new ice production (e.g. Cheng et al., 2017). However, the ASP may close both due to ice production
591 and movement of previously-produced ice into the polynya. Second, we suggest that the blockages of ice in the vi-
592 cinity of the polynya reduce the size and frequency of polynya events by hindering the ability of ice to move out of
593 the polynya and open it up. Again, by reducing the size and duration of open polynya area during winter, ice produc-
594 tion is limited.

595 We also note that the ASP forms along the coast westward off a chain of icebergs that extend from the
596 Thwaites Iceberg Tongue. While some polynyas, such as the Ross Ice Shelf polynya, form off and away from the
597 coast, the majority of Antarctic polynyas have been shown to form westward off glacier ice tongues or protruding



598 fast ice (Nihashi et al., 2017). In the case of the ASP, its location and orientation is determined by the presence of
599 the ‘Iceberg Chain’, which is in turn determined by the presence of a bathymetric high (Figs. 1-2). Stammerjohn et
600 al. (2015) refer to the polynya as forming off a ‘fast ice tongue’ but we prefer to refer to the ‘Iceberg Chain’ as the
601 eastern boundary. While a section of fast ice exists amongst, and adjacent to, a section of the southern part of the
602 Iceberg Chain, the extent of this fast ice varies and it only ever extends along a portion of the Iceberg Chain. The
603 Iceberg Chain remains virtually the same length throughout our observations. The polynya consistently forms off the
604 Iceberg Chain regardless of the state or extent of the fast ice. This means that, unlike polynyas that form off variable
605 fast ice (Nihashi et al., 2017), the fundamental morphology of the ASP remains stable through the period. We also
606 note that at no point do we observe significant portions of icepack to ‘break through’ the Iceberg Chain from the
607 east, regardless of the state of fast ice extent or conditions, and thus the icebergs and the bathymetric high persistent-
608 ly ‘shield’ the polynya from icepack inflow.

609 Another notable feature of the ASP is the development of a ‘secondary polynya’ during the winter (Fig.
610 2a), where ice production also takes place. This is a polynya that forms within the ASP study area, in an area that is
611 usually part of the main ASP during the summer, but it is not typically congruent with the ‘main’ polynya during the
612 winter. The polynya forms at the site of the ‘Central Grounded Icebergs’ and associated ‘stuck’, transient fast ice.
613 Because some ice has become stuck over the bathymetric high, when adjacent ice drifts away, a polynya opens. This
614 feature again highlights the significance of the bathymetry of the region for sea ice production and dynamics.

615 In line with previous studies of the ASP we find that the ASP is an important site of ice production
616 throughout the winter. Our estimates of annual ice production for 2019 and the mean for 2017-20 fall within the
617 range of predictions by Tamura et al. (2008; 2016) and Ohshima et al. (2017) for 1992-2001/2003-10/2013-15 (90 -
618 117km³) (Fig. 7). Our estimates for total annual ice production for 2017 (139 km³) and 2018 (121 km³) are higher
619 than the highest estimate of those studies, while for 2020 (80 km³) it is lower. This suggests no significant trend in
620 interannual ice production can be discerned from comparing the period of our study to these previous studies. Some
621 caution must be used in this comparison, however, because those studies include March in ice production calcula-
622 tions and our ASP study area does not exactly correspond to theirs.

623 We find that the shoulder seasons of April/May and September/October are particularly important for ice
624 production due to the higher polynya area at these times, accounting for 36% and 42% of the annual ice production,
625 respectively. This is particularly the case in 2017, when an exceptionally high open polynya area in the summer, due
626 to low icepack conditions (discussed below), continues into the winter period (Figs. 5-7). However, we show that at
627 least some polynya area opens and some ice production occurs throughout the whole winter (Figs. 6-7). Addition-
628 ally, there can be spikes in polynya area and ice production in the deepest winter months. Most notably, polynya area
629 reaches 26 631 km² in June. Such isolated, winter events are not reflected in the daily mean for the whole study pe-
630 riod, but only when analyzing daily changes for each year (Fig. 6), highlighting the importance of analyzing polynya
631 area and ice production at the daily scale to discern important polynya dynamics.

632 When comparing our results to those of Cheng et al. (2017), who used the same method for calculating ice
633 production at the Ross Ice Shelf Polynya, we find that the ASP produces substantially less ice. Between 2003 and
634 2015 they found ice production for the Ross Ice Shelf Polynya was between 164 and 313 km³ (also for April - Octo-



635 ber) compared to 80 to 139 km³ for the Amundsen Sea Polynya (this study). This is in line with other studies that
636 compare the two polynyas (Tamura et al. 2008; 2016; Nihashi et al. 2017). We suggest that one limit on polynya
637 area and ice production for the ASP compared to the larger Ross Ice Shelf Polynya, is that the ASP typically forms
638 off the Iceberg Chain. The Iceberg Chain has a stable length of ~190 km, limited by the length of the seafloor sill on
639 which it is grounded, and is an upper limit on the polynya in one dimension. The Ross Ice Shelf Polynya, on the
640 other hand, forms off a coastline, and is only typically limited in this spatial dimension by weather/oceanographic
641 conditions. Another comparative limit on the ASP's ice production is the previously discussed tendency for polyn-
642 ya-produced ice to inhibit further opening of the polynya due to blockages and reversals in ice drift. This process
643 could also partly explain why Cheng et al. (2017) found ice production to remain relatively consistent throughout
644 the winter for the Ross Ice Shelf Polynya, whereas we find ice production for the ASP in June-August to be much
645 lower than in the shoulder months of April/May and September/October.

646 We also note the polynya-produced ice leaves our study area and enters the adjacent sector of the Amund-
647 sen Sea to the west, rather than traveling away from the coast after formation. This westward flow of the ice away
648 from the polynya is likely, in this section, primarily due to the prevalence of easterly winds, especially towards the
649 western part of the study area, and westward ocean currents in the region (Kim et al., 2016; St-Laurent et al., 2019).
650 These ocean currents have been shown to carry icebergs away from our study region, westward through the Amund-
651 sen Sea and into the Ross Sea (Koo et al., 2021). Broader prevailing easterly winds likely play a dominant role in
652 sea ice produced by the ASP eventually drifting to the Ross Sea, as part of a coastal band of westward ice drift
653 (Assmann et al., 2005). The fact that the polynya-produced ice remains by the coast may also be influenced by the
654 inflow of older, thicker icepack into our study area. Icepack appears to flow into the region from the Bellingshausen
655 Sea (Video S1, S2) and flows parallel to the ASP-produced ice, potentially playing some role in 'trapping' the ice by
656 the coast. The westward flow of the ice suggests that the level of ice production in the ASP is significant for the ad-
657 jacent sector of the Amundsen Sea and the Ross Sea.

658 During the summer we observe the ASP to behave in a similar way in 2016/17 - 2020/21 as Stammerjohn
659 et al. (2015) showed for the period 1979 - 2014. As they did, we find the polynya to open every summer during our
660 study period. We do not note any shift in the location of opening, with the location remaining in the same place as
661 Stammerjohn et al. (2015) noted that it had shifted to in 1992/93. As they did for the years 1992, 1993, 1995, 1997,
662 2003, and 2010, we also note that in 2016/17, there is no icepack adjacent to the ASP in the north and west. This is
663 due to limited advection from the Bellingshausen Sea and Pine Island Polynya, and it causes the ASP to become
664 congruent with the open ocean (Fig. 11). This year was noted as a year of unprecedented springtime retreat and low
665 sea ice concentration for Antarctic sea ice, and was associated with a series of record atmospheric circulation anom-
666 alies and sea surface temperatures (Turner et al., 2017). These broader sea ice conditions caused the polynya to be
667 open in approximately the whole ASP study area through most of the summer in 2016/17, from late November to
668 March. During this time there is also little-to-no distinction between the ASP and the neighboring Pine Island Po-
669 lynya, other than the presence of the Iceberg Chain (Fig. 11a, Video S1). The effect of these extraordinary sea ice
670 conditions in 2016/17 on the polynya in summer, and early winter as mentioned above, may offer insight into how
671 the ASP will behave more commonly in future if climate change makes such conditions more likely.



672 We note that while Stammerjohn et al. (2015) found the largest polynya area to be February in all but two
673 years during 1979 - 2014, we find the polynya area to be highest in January in each year apart from 2016/17 (when it
674 reaches the peak in November) (Fig. 5). Arrigo et al. (2012) also generally found the polynya area to increase until a
675 later peak in February for the years 1997/98 - 2009/10. While there should be some caution in directly comparing
676 our results with those, due to varying datasets, methods and definitions of the study area, we suggest that a shift in
677 the timing of maximum summer area would promote primary productivity in the polynya. Arrigo et al. (2012) found
678 primary productivity (per unit area) to typically peak in January, and to be declining by the time of the polynya area
679 peak. If the polynya reaches a higher area at an earlier time, when primary productivity is higher, we suggest the
680 potential for primary productivity may be larger during our study period.

681

682 **6. Conclusions**

683 Focusing on the summers of 2016/17 - 2020/21 and the winters of 2017 - 2020, we present the first detailed
684 study of year-round variations in the Amundsen Sea Polynya's behavior, area, and ice production. In particular, we
685 take advantage of the recent availability of Sentinel-1 SAR imagery to qualitatively assess the dynamics of the po-
686 lynya through the whole year.

687 Our findings agree with previous studies of earlier periods in finding that the ASP produces a substantial
688 amount of ice through the winter, with some inter-annual variation. We add that the shoulder seasons of April/May
689 and September/October dominate winter ice production, contributing a combined 78%. However, large polynya
690 events, often associated with high winds, can occur throughout the winter, promoting significant ice production.

691 The ASP opens each summer in November and closes in March or early April, with peak area typically
692 occurring in January. We find that broader regional sea ice conditions can play an important role in the polynya in
693 summer, with the record-low sea ice extent in 2016/17 causing the ASP to become part of the open ocean to the
694 north and join with the Pine Island Polynya to the east.

695 Through our qualitative assessment we identify that the ASP behaves in a distinct manner. The polynya
696 typically forms in a westward direction off a persistent chain of grounded icebergs that are grounded along a bathy-
697 metric high. Ice produced by the polynya is not efficiently evacuated from the site as with other polynyas such as the
698 Ross Ice Shelf Polynya. Instead it stays within the study site, typically for months through the winter, sometimes
699 becoming stuck. This behavior is related to local topographic sea-floor highs which cause icebergs to become
700 grounded and ice to become stuck. At times another smaller 'secondary polynya' forms within the study area adja-
701 cent to grounded icebergs. Relatedly, ice produced by the polynya does not consistently move away from the ASP,
702 instead 'heaving' and sometimes drifting back towards it, contributing to its closure and limiting ice production.
703 Unlike some other polynyas, the polynya-produced ice also drifts westward into other sectors, instead of north, away
704 from the coast. These behaviors should be accounted for when considering the ASP's influence on the region's sea
705 ice, biology and oceanography.

706 Given temporal and spatial gaps in Sentinel-1 SAR's coverage, we do not find that it can replace passive
707 microwave or sea ice concentration datasets for analyzing daily changes in polynya area or ice production. However,
708 we find that the ability to directly observe and qualitatively analyze the polynya at a high spatial and temporal reso-



709 lution, year-round, with Sentinel-1 imagery provides important insights that are not possible with those other da-
710 taset. We also note that it is sometimes possible to visually-track ice created by particular polynya events for sever-
711 al months as it drifts. Employing ice-tracking algorithms to track ice produced by polynya events in Sentinel-1 im-
712 ages, with measurements of ice thickness (e.g. from satellite altimetry), could help further quantify ice production by
713 polynyas and extract more potential from Sentinel-1 datasets.

714

715 *Code and Data Availability*

716 Code for data processing and production of figures and videos is available at
717 <https://github.com/georgeordie/AmundsenSeaPolynyaPaper>. All processing was done with freely available software,
718 and all data is freely available. Sentinel-1 images were processed in Google Earth Engine or downloaded from:
719 asf.alaska.edu. BedMachine Antarctica V2 was downloaded from: <https://nsidc.org/data/nsidc-0756>. Sea ice concen-
720 tration data was downloaded from: <http://seaice.uni-bremen.de/>. ERA5 climate data was downloaded from:
721 <https://cds.climate.copernicus.eu>. The MODIS image used for Fig. 1b was downloaded from:
722 <https://worldview.earthdata.nasa.gov/>

723

724 *Video Supplement*

725 Video S1: <https://doi.org/10.5281/zenodo.5179444>
726 Video S2: <https://doi.org/10.5281/zenodo.5179509>
727 Video S3: <https://doi.org/10.5281/zenodo.5179590>

728

729 *Author Contributions*

730 GJM primarily conceived the study, processed and analyzed all data and produced all figures. SFA and AMM-N
731 also contributed to the design of the study and all authors discussed the results and were involved in editing the
732 manuscript.

733

734 *Competing Interests*

735 The authors declare that they have no conflict of interest.

736

737 *Financial Support*

738 This work was supported by NASA grant #80NSSC19M0194.

739

740 *Acknowledgements*

741 We gratefully acknowledge the European Space Agency for making available Sentinel-1 data and the SNAP
742 toolbox, and Google Earth Engine for hosting and processing Sentinel-1 data. We acknowledge the free package
743 Quantarctica, developed by the Norwegian Polar Institute, for use in Fig. 1a. We thank the University of Bremen
744 Sea Ice Remote Sensing Group for processing and making available their sea ice concentration product and the Jap-
745 anese Space Exploration Agency for launching and managing AMSR2. We also acknowledge the ECMWF, NSIDC



746 and NASA for freely-available data. Among others, the free, open-source software packages QGIS, GDAL, Python,
747 NumPy and Matplotlib were invaluable in this research. We also thank the GIS and StackOverflow StackExchange
748 communities for resources that aided data processing. We thank three anonymous reviewers who reviewed an earlier
749 draft of this paper and editor Nicolas Jourdain for suggested minor revisions.

750

751 **References**

752 Armstrong, T.: World meteorological organization: WMO sea-ice nomenclature. Terminology, codes and illustrated
753 glossary. *J. Glaciol.*, 11, 148–149. <https://doi.org/10.3189/S0022143000022577>, 1972.

754
755 Arrigo, K. R., van Dijken, G. L., and Bushinsky, S.: Primary production in the Southern Ocean, 1997–2006, *J. Geophys. Res.*,
756 113, C08004. <https://doi.org/10.1029/2007JC004551>, 2008a.

757
758 Arrigo, K. R., van Dijken, G. L., and Long, M.: Coastal Southern Ocean: A strong anthropogenic CO₂ sink. *Geophys. Res. Lett.*,
759 35, L21602. <https://doi.org/10.1029/2008GL035624>, 2008b.

760
761 Arrigo, K. R., Lowry, K. E., and van Dijken, G. L.: Annual changes in sea ice and phytoplankton in polynyas of the
762 Amundsen Sea, Antarctica. *Deep Sea Research, II* 71–76: 5–15. <https://doi.org/10.1016/j.dsr2.2012.03.006>, 2012.

763
764 Arrigo, K. R. and van Dijken, G. L.: Phytoplankton dynamics within 37 Antarctic coastal polynya systems. *J. Geophys. Res.*,
765 108, 3271 <https://doi.org/10.1029/2002jc001739>, 2003.

766
767 Arthur, J. F., Stokes, C. R., Jamieson, S. S. R., Miles, B. W. J., Carr, J. R., and Leeson, A. A.: The triggers of the dis-
768 aggregation of Voyeykov Ice Shelf (2007), Wilkes Land, East Antarctica, and its subsequent evolution. *J. Glaciol*
769 <https://doi.org/10.1017/jog.2021.45>, 2021.

770
771 Assmann, K. M., Hellmer, H. H., and Jacobs, S. S.: Amundsen Sea ice production and transport. *J. Geophys. Res.*,
772 110, C12013. <https://doi.org/10.1029/2004JC002797>, 2005.

773
774 Banwell, A. F., Willis, I. C., Macdonald, G. J., Goodsell, B., Mayer, D. P., Powell, A., and MacAyeal, D. R.: Calving
775 and rifting on the McMurdo Ice Shelf, Antarctica. *Ann. Glaciol.*, 58, 78–87. <https://doi.org/10.1017/aog.2017.12>,
776 2017.

777
778 Bett, D. T., Holland, P. R., Naveira Garabato, A. C., Jenkins, A., Dutrieux, P., Kimura, S., and Fleming, A.: The
779 impact of the Amundsen Sea freshwater balance on ocean melting of the West Antarctic Ice Sheet. *J. Geophys. Res.: Oceans*,
780 125, e2020JC016305. <https://doi.org/10.1029/2020JC016305>, 2020.

781
782 Bracegirdle, T. J.: Climatology and recent increase of westerly winds over the Amundsen Sea derived from six reanalyses.
783 *Int. J. Climatol.*, 33, 843–851. <https://doi.org/10.1002/joc.3473>, 2013.

784
785 Bromwich, D. H. and Kurtz, D. D.: Katabatic wind forcing of the Terra Nova Bay polynya. *J. Geophys. Res.*, 89,
786 3561. <https://doi.org/10.1029/JC089iC03p03561>, 1984.

787
788 Bromwich, D., Liu, Z., Rogers, A. N., and Van Woert, M. L.: Winter atmospheric forcing of the Ross Sea polynya.
789 *Ocean ICE Atmos. Int. Antarct. Cont. Margin*, 75, 101–133. <https://doi.org/10.1029/AR075p0101>, 1998.

790
791 Bromwich, D. H., Carrasco, J. F., Liu, Z., and Tzeng, R. Y.: Hemispheric atmospheric variations and oceanographic
792 impacts associated with katabatic surges across the ross ice shelf, Antarctica. *J. Geophys. Res.-Atmos*, 98, 13045–
793 13062. <https://doi.org/10.1029/93JD00562>, 1993.

794 Budge, J. S. and Long, D. G.: A comprehensive database for Antarctic iceberg tracking using scatterometer data.
795 *IEEE JSTARS* 11(2), 434–442. <https://doi.org/10.1109/JSTARS.2017.2784186>, 2018.

796
797 Cheng, Z., Pang, X., Zhao, X., and Tan, C.: Spatio-Temporal Variability and Model Parameter Sensitivity Analysis
798 of Ice Production in Ross Ice Shelf Polynya from 2003 to 2015. *Remote Sensing*, 9, 934.



- 799 <https://doi.org/10.3390/rs9090934>, 2017.
800
801 Cheng, Z., Pang, X., Zhao, X., and Stein, A.: Heat Flux Sources Analysis to the Ross Ice Shelf Polynya Ice Produc-
802 tion Time Series and the Impact of Wind Forcing, *Remote Sensing*, 11, 188. <https://doi.org/10.3390/rs11020188>,
803 2019.
804
805 Dai, L., Xie, H., Ackley, S. F., and Mestas-Nuñez, A. M.: Ice Production in Ross Ice Shelf Polynyas during 2017–
806 2018 from Sentinel–1 SAR Images. *Remote Sensing*, 12, 1484. <https://doi.org/10.3390/rs12091484>, 2020.
807
808 Doherty, B. T. and Kester, D. R.: Freezing Point of Seawater. *J. Mar. Res.*, 32, 285–300. 1974.
809
810 Drucker, R., Martin, S., and Kwok, R.: Sea ice production and export from coastal polynyas in the Weddell and
811 Ross Seas. *Geophys. Res. Lett.*, 38, L1705. <https://doi.org/10.1029/2011GL048668>, 2011.
812
813 Greene, C. E., Young, D. A., Gwyther, D. E., Galton-Fenzi, B. E., and Blankenship, D. D.: Seasonal dynamics of
814 Totten Ice Shelf controlled by sea ice buttressing. *Cryosphere*, 12, 2869–2882. [https://doi.org/10.5194/tc-12-2869-](https://doi.org/10.5194/tc-12-2869-2018)
815 [2018](https://doi.org/10.5194/tc-12-2869-2018), 2018.
816
817 Grossmann, S. and Dieckmann, G. S.: Bacterial Standing Stock, Activity, and Carbon Production during Formation
818 and Growth of Sea–Ice in the Weddell Sea, Antarctica. *Appl. Environ. Microb.*, 60, 2746–2753.
819 <https://doi.org/10.1128/aem.60.8.2746-2753.1994>, 1994.
820
821 Hersbach, H., Bell, B., Berrisford, P., Biavati, G., Horányi, A., Muñoz Sabater, J., Nicolas, J., Peubey, C., Radu, R.,
822 Rozum, I., Schepers, D., Simmons, A., Soci, C., Dee, D., and Thépaut, J.-N.: ERA5 monthly averaged data on single
823 levels from 1979 to present. Copernicus Climate Change Service (C3S) Climate Data Store (CDS). (Accessed on <
824 01-04-2021), <https://doi.org/10.24381/cds.fl7050d7>, 2019.
825
826 Hollands, T. and Dierking, W.: Dynamics of the Terra Nova Bay Polynya: The potential of multi-sensor satellite
827 observations, *Remote Sens. Environ.*, 187, 30–48, <https://doi.org/10.1016/j.rse.2016.10.003>, 2016
828
829 IMBIE team: Mass balance of the Antarctic ice sheet from 1992 to 2017. *Nature* 558, 219–222.
830 <https://doi.org/10.1038/s41586-018-0179-y>, 2018.
831
832 Ito, M., Ohshima, K. I., Fukamachi, Y., Mizuta, G., Kusumoto, Y., and Nishioka, J.: Observations of frazil ice for-
833 mation and upward sediment transport in the Sea of Okhotsk: A possible mechanism of iron supply to sea ice. *J.*
834 *Geophys. Res.–Oceans*, 122, 788–802. <https://doi.org/10.1002/2016JC012198>, 2017.
835
836 Kim, C.-S., Kim, K.-W., Cho, K.-H., Ha, H. K., Lee, S.H., Kim, H.-C., Lee, J.-H.: Variability of the Antarctic
837 Coastal Current in the Amundsen Sea. *Estuar. Coast. Shelf S.*, 181, 123–133,
838 <https://doi.org/10.1016/j.ecss.2016.08.004>, 2016.
839
840 Kimura, N. and Wakatsuchi, M.: Increase and decrease of sea ice area in the Sea of Okhotsk: Ice production in
841 coastal polynyas and dynamic thickening in convergence zones. *J. Geophys. Res.-Oceans*, 109, C09S03.
842 <https://doi.org/10.1029/2003JC001901>, 2004.
843
844 Koo, Y., Xie, H., Ackley, S. F., Mestas-Nuñez, A. M., Macdonald, G. J., and Hyun, C.-U.: Semi-automated tracking
845 of iceberg B43 using Sentinel-1 SAR images via Google Earth Engine. *Cryosphere.*, 15, 4727–4744,
846 <https://doi.org/10.5194/tc-15-4727-2021>, 2021.
847
848 Lee, S.H., Hwang, J., Ducklow, H. W., Hahm, D., Lee, S. H., Kim, D., Hyun, J.-H., Park, J., Ha, H. K., Kim, T. W.,
849 Yang, E. J., Shin, H. C.: Evidence of minimal carbon sequestration in the productive Amundsen Sea polynya, *Ge-*
850 *ophys. Res. Lett.*, 44, 15, 7892–7899. <https://doi.org/10.1002/2017GL074646>, 2017.
851
852 Massom, R. A., Hill, K. L., Lytle, V. I., Worby, A.P., Paget, M. J., and Allison, I.: Effects of regional fast-ice and
853 iceberg distributions on the behaviour of the Mertz Glacier polynya, East Antarctica. *Ann. Glaciol.*, 33, 391–398.
854 <https://doi.org/10.3189/172756401781818518>, 2001.



- 855
856 Massom, R. A., Scambos, T. A., Bennetts, L. G., Reid, P., Squire, V. A., and Stammerjohn, S. E.: Antarctic ice shelf
857 disintegration triggered by sea ice loss and ocean swell. *Nature*, 558, 383-389. [https://doi.org/10.1038/s41586-018-](https://doi.org/10.1038/s41586-018-0212-1)
858 [0212-1](https://doi.org/10.1038/s41586-018-0212-1), 2018.
- 859
860 Matsuoka, K., Skoglund, A., Roth, G., de Pomereu, J., Griffiths, H., Headland, R., Herried, B., Katsumata, K., Le
861 Brocq, A., Licht, K., Morgan, F., Neff, P. D., Ritz, C., Scheinert, M., Tamura, T., Van de Putte, A., van den Broeke,
862 M., von Deschanden, A., Deschamps-Berger, C., Van Liefferinge, B., Tronstad, S., and Melvær, Y.: Quantarctica,
863 an integrated mapping environment for Antarctica, the Southern Ocean, and sub-Antarctic islands. *Environ. Modell.*
864 *Softw.*, 140, 105015. <https://doi.org/10.1016/j.envsoft.2021.105015>, 2021.
- 865
866 Mazur, A. K., Wåhlin, A. K., Krężel, A.: An object-based SAR image iceberg detection algorithm applied to the
867 Amundsen Sea, *Remote Sens. Environ.*, 189, 67–83, <https://doi.org/10.1016/j.rse.2016.11.013>, 2017.
- 868
869 Mazur, A. K., Wåhlin, A. K., and Kalén, O.: The life cycle of small-to medium-sized icebergs in the Amundsen sea
870 embayment, *Polar Res.*, 38, 1–17, <https://doi.org/10.33265/polar.v38.3313>, 2019.
- 871
872 Morales Maqueda, M. A., Willmott, A. J., and Biggs, N. R. T.: Polynya dynamics: a review of observations and
873 modeling, *Review of Geophysics*, 42, RG1004. <https://doi.org/10.1029/2002RG000116>, 2004.
- 874
875 Morelli, S. and Parmiggiani, F.: Wind over Terra Nova Bay (Antarctica) during a polynya event: Eta model simula-
876 tions and satellite microwave observations. *Eur. Phys. J. Plus* 128, 135 (2013). [https://doi.org/10.1140/epj/i2013-](https://doi.org/10.1140/epj/i2013-13135-8)
877 [13135-8](https://doi.org/10.1140/epj/i2013-13135-8), 2013.
- 878
879 Morlighem, M.: MEaSURES BedMachine Antarctica, Version 2. Boulder, Colorado USA. NASA National Snow
880 and Ice Data Center Distributed Active Archive Center. <https://doi.org/10.5067/C2GFER6PTOS4>, 2019. [Date Ac-
881 cessed: 01-04-2021].
- 882
883 Nihashi, S., and Ohshima, K. I.: Circumpolar Mapping of Antarctic Coastal Polynyas and Landfast Sea Ice: Rela-
884 tionship and Variability, *J. Climate*, 28, 3650-3670. <https://doi.org/10.1175/JCLI-D-14-00369.1>, 2015.
- 885
886 Nihashi, S., Ohshima, K. I., and Tamura, T.: Sea-Ice Production in Antarctic Coastal Polynyas Estimated From
887 AMSR2 Data and Its Validation Using AMSR-E and SSM/I-SSMIS Data. *IEEE JSTARS*, 10, 3912-3922.
888 <https://doi.org/10.1109/JSTARS.2017.2731995>, 2017.
- 889
890 Ohshima, K. I., Fukamachi, Y., Williams, G. D., Nihashi, S., Roquet, F., Kitade, Y., Tamura, T., Hirano, D., Her-
891 raiz-Borreguero, L., Field, I., Hindell, M., Aoki, S. and Wakatsuchi, M. L.: Antarctic Bottom Water production by
892 intense sea-ice formation in the Cape Damley polynya. *Nat. Geosci.*, 6, 235-240. <https://doi.org/10.1038/ngeo1738>,
893 2013.
- 894
895 Park, J., Kim, H.-C., Jo, Y.-H., Kidwell, A., and Hwang, J.: Multi-temporal variation of the ross sea polynya in re-
896 sponse to climate forcings. *Polar Res.*, 37, 1444891. <https://doi.org/10.1080/17518369.2018.1444891>, 2018.
- 897
898 Parkinson, C. L.: A 40-y record reveals gradual Antarctic sea ice increases followed by decreases at rates far exceed-
899 ing the rates seen in the Arctic. *P. Natl. Acad. Sci. U.S.A.*, 116, 14414-14423.
900 <https://doi.org/10.1073/pnas.1906556116>, 2019.
- 901
902 Parmiggiani, F.: Fluctuations of Terra Nova Bay polynya as observed by active (ASAR) and passive (AMSR-E)
903 microwave radiometers, *Int. J. Remote. Sens.*, 27:12, 2459 2467. <https://doi.org/10.1080/01431160600554355>,
904 2007.
- 905
906 Preußner, A., Heinemann, G., Willmes, S., and Paul, S.: Multi-Decadal Variability of Polynya Characteristics and Ice
907 Production in the North Water Polynya by Means of Passive Microwave and Thermal Infrared Satellite Imagery.
908 *Remote Sensing*, 7, 15844-15867. <https://doi.org/10.3390/rs71215807>, 2015.
- 909
910 [QGIS.org](http://www.qgis.org): QGIS Geographic Information System. QGIS Association. <http://www.qgis.org>. 2021.



- 911
912 Rack, W., Price, D., Haas, C., Langhorne, P. J., and Leonard, G. H.: Sea Ice Thickness in the Western Ross Sea.
913 *Geophys. Res. Lett.*, 48, e2020GL090866. <https://doi.org/10.1029/2020GL090866>, 2020.
914
915 Rignot, E., Mouginot, J., Scheuchl, B., van den Broeke, M., van Wessem, M. J., and Morlighem, M.: Four decades
916 of Antarctic ice sheet mass balance from 1979–2017. *P. Natl. Acad. Sci. U.S.A.* 116, 1095–1103.
917 <https://doi.org/10.1073/pnas.1812883116>, 2019.
918
919 Sansiviero, M., Morales Maqueda, M. Á., Fusco, G., Aulicino, G., Flocco, D., and Budillon, G.: Modelling sea ice
920 formation in the Terra Nova Bay polynya. *J. Marine Syst.*, 166, 4–25. <https://doi.org/10.1016/j.jmarsys.2016.06.013>,
921 2017.
922
923 Spreen, G., Kaleschke, G. L., and Heygster, G.: Sea ice remote sensing using AMSR-E 89 GHz channels. *J. Geophys.*
924 *Res.*, 113, C02S03. <https://doi.org/10.1029/2005JC003384>, 2008.
925
926 Stammerjohn, S. E., Maksym, T., Massom, R. A., Lowry, K. E., Arrigo, K. R., Yuan, X., Raphael, M., Randall-
927 Goodwin, E. R., Sherrell, R. M., and Yager, P. L.: Seasonal sea ice changes in the Amundsen Sea, Antarctica, over
928 the period of 1979–2014. *Elementa: Science of the Anthropocene*, 3, 000055.
929 <https://doi.org/10.12952/journal.elementa.000055>, 2015.
930
931 St-Laurent, P., Yager, P. L., Sherrell, R. M., Stammerjohn, S. E., and Dinniman, M. S.: Pathways and supply of dis-
932 solved iron in the Amundsen Sea (Antarctica). *J. Geophys. Res.-Oceans*, 122, 7135–7162, [https://doi.org/10.1002/](https://doi.org/10.1002/2017JC013162)
933 [2017JC013162](https://doi.org/10.1002/2017JC013162), 2017.
934
935 St-Laurent, P., Yager, P. L., Sherrell, R. M., Oliver, H., Dinniman, M. S., and Stammerjohn, S. E.: Modeling the
936 seasonal cycle of iron and carbon fluxes in the Amundsen Sea Polynya, Antarctica. *J. Geophys. Res.: Oceans*, 124,
937 1544–1565. <https://doi.org/10.1029/2018JC014773>, 2019.
938
939 Sweeney, C.: The annual cycle of surface water CO₂ and O₂ in the Ross Sea: A model for gas exchange on the con-
940 tinental shelves of Antarctica, in *Biogeochemistry of the Ross Sea. Antarctica Research Series*, 78, edited by Dun-
941 bar, R. B., and DiTullio, G. R., pp. 295–312, AGU, Washington, D. C., 2003.
942
943 Tamura, T., Ohshima, K. I., and Nihashi, S.: Mapping of sea ice production for Antarctic coastal polynyas, *Ge-*
944 *ophys. Res. Lett.*, 35, L07606. <https://doi.org/10.1029/2007GL03290>, 2008.
945
946 Tamura, T., Williams, G. D., Fraser, A. D., and Ohshima, K. I.: Potential regime shift in decreased sea ice produc-
947 tion after the Mertz Glacier calving. *Nat. Commun.*, 3, 826. <https://doi.org/10.1038/ncomms1820>, 2012.
948
949 Tian, L., Xie, H., Ackley, S. F., Tang, J., Mestas-Núñez, A. M., and Wang, X.: Sea-ice freeboard and thickness in
950 the Ross Sea from airborne (IceBridge 2013) and satellite (ICESat 2003–2008) observations. *Ann. Glaciol.*, 61(82),
951 24–39. <https://doi.org/10.1017/aog.2019.49>, 2020.
952
953 Webber, B. G. M., Heywood, K. J., Stevens, D. P., Dutrieux, P., Povel Abrahamsen, E., Jenkins, A., Jacobs, S. S.,
954 Ha, H. K., Lee, S. H., and Kim, T. W.: Mechanisms driving variability in the ocean forcing of Pine Island Glacier,
955 *Nat. Commun.*, 8, 14507. <https://doi.org/10.1038/ncomms14507>, 2017.